Multiple excitable signaling dynamics regulate pseudopod formation in eukaryotic chemotaxis

Submitted to Department of Biological Science,
Graduate School of Science, Osaka University

May 5, 2020

Yuki TANABE

Abstract

In eukaryotic chemotaxis, parallel signaling pathways regulate the spatio-temporal pseudopod dynamics at the leading edge of a motile cell. Chemotactic signaling pathways have an excitable characteristic. However, differences in the excitability and the physiological roles of individual pathways remain to be elucidated. Here I found that two pathways in *Dictyostelium discoideum*, soluble guanylyl cyclase (sGC) and phosphatidylinositol (3,4,5)-triphosphate (PIP3), exhibited similar all-or-none responses but different refractory periods by simultaneously observing their excitable properties. sGC signaling responded more frequently to a chemoattractant, leading to pseudopod formation with higher frequency because of the shorter refractory period than PIP3. sGC excitability was regulated negatively by its catalytic product, cGMP, and cGMP-binding protein C (GbpC) through the suppression of F-actin polymerization, providing the underlying delayed negative feedback mechanism for the cyclical pseudopod formation. Additionally, sGC itself binds to and crosslinks F-actin in vitro, suggesting that sGC regulates both the positive and negative feedback that constitute an excitable system. These results indicate that parallel pathways respond on different time scales to environmental cues for chemotactic motility based on their intrinsic excitability.

Abbreviations

cAMP	Cyclic adenosine monophosphate
cGMP	Cyclic guanosine monophosphate
Gbp	cGMP-binding protein
GFP	Green fluorescent protein
LatA	Latrunculin A
PHD	Pleckstrin homology domain
PI3K	Phosphoinositide 3-kinase
PIP2	Phosphatidylinositol (4,5)-biphosphate
PIP3	Phosphatidylinositol (3,4,5)-triphosphate
PKB	Protein kinase B
PTEN	Phosphatase and tensin homolog
RFP	Red fluorescent protein
Rh-Ph	Rhodamine-Phalloidin
sGC	Soluble guanylyl cyclase
TMR	Tetramethylrhodamine
TorC	Target of rapamycin complex
WCE	Whole cell extract

Contents

Chapter 1

Introduction

1.1 Cell migration in eukaryotic cells

Chemotaxis, the directed cell migration in response to extracellular chemical signals, plays important roles in various physiological phenomena including neurogenesis, immune response and wound healing [22], [33], [44]. Chemotactic cells such as mammalian neutrophils and social amoeba *Dictyostelium discoideum* detect chemical gradients and migrate directionally by coordinating their anterior pseudopod formation and posterior tail contraction [18], [55]. These morphological changes are induced by the structural transitions of cytoskeletal proteins such as actin and myosin, transitions that are produced by an asymmetric localization pattern of signaling molecules [2], [11]. The symmetry breaking of signaling localization and pseudopod formation are occurred even in the absence of chemoattractant, which is similar to that induced by external stimulus [19], [62]. Thus, it is considered that the fluctuation of signaling activity produces the spontaneous localization of signaling molecule, resulting in pseudopod formation.

Pseudopod has very fast dynamics and proceeds within seconds to minutes. Thus, the cell can respond abruptly to changes in the external environment, as seen with *Dictyostelium* cell reactions to changes in chemoattractant concentrations [36], [51]. On the other hand, too fast a response to external signals can cause errors in the migration direction. In other words, fast responsiveness and accuracy are in conflict, the so-called speed-accuracy trade-off [31], [47]. How cells balance them by regulating their anterior and posterior sides is almost never discussed.

1.2 Chemotactic signal transduction network

Cells sense changes of the external environment at the cell membrane, and evolutionally conserved molecular networks drive cell migration [2], [10]. In *Dictyostelium* cells, extracellular cAMP is detected by G protein coupled receptor (GPCR) and heterotrimeric G-proteins as the chemoattractant. cAMP activates multiple downstream signaling pathways including PI3K-PTEN, PLA2, TorC2-PDK-PKB and sGC (Fig. 1.1). These signaling pathways promote actin polymerization at the higher side of the cAMP concentration and myosin retraction at the lower side. Some studies have revealed that multiple pathways mediate chemotaxis in parallel because only one of them is sufficient for significant chemotaxis in steep gradients [2], [8], [10]. On the other hand, multiple pathways enhance the accuracy of the chemotactic migration compared to a single pathway in shallow cAMP gradients [59].

Among multiple pathways, the PI3K-PTEN pathway is well studied. cAMP stimulation induces PI3K activation and the production of phosphatidylinositol 3,4,5-trisphosphate (PIP3). At the higher side of the cAMP concentration, the PIP3-enriched domain localizes to the pseudopod and regulates the polymerization or stabilization of F-actin [10], [27]. Inhibition of PI3K activation by genetic or pharmacological treatment introduced that cell cannot produce PIP3 and shows the decrease in migration velocity and chemotactic efficiency [42], [50]. On the other hand, PTEN molecules dephosphorylate PIP3 to PIP2, which suppresses pseudopod formation at the posterior side. Mutant cell lacking PTEN exhibited the elevated PIP3 levels and more pseudopod formation [21].

Pseudopod formation is occurred even in the absence of chemoattractant and cell extends a new pseudopod in a random direction [37]. PIP3-enriched domain is generated in the restricted region on the cell membrane, which is coupled with pseudopod formation. Similar localizations of sGC and PKB also act as intracellular cues for pseudopod formation [23], [57]. However, whether functional differences among the several pathways exist is unclear. Thus, it is important to research the localization dynamics of each pathway in order to understand how pseudopod formation is regulated by multiple pathways in a single cell.

Fig. 1.1

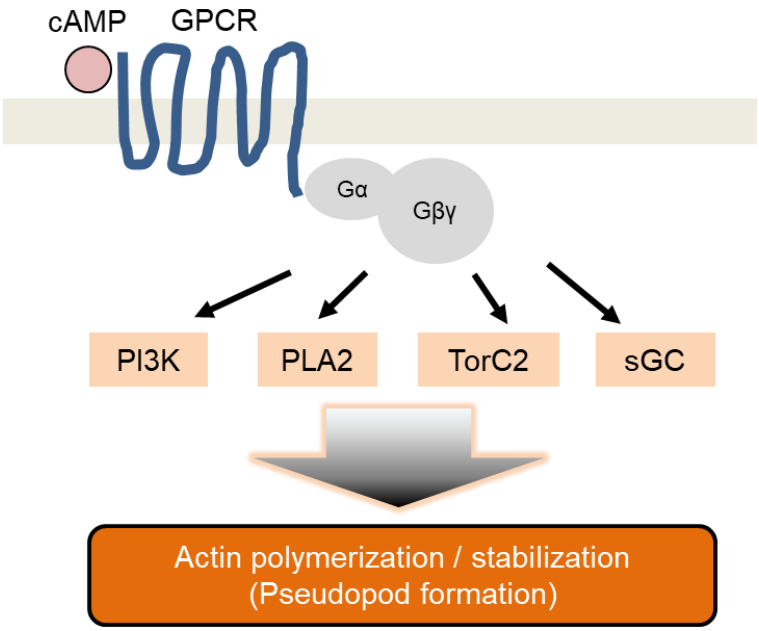

Fig. 1.1 Parallel pathways regulating chemotaxis in *Dictyostelium* cells.
cAMP binding to GPCR is translated into the intracellular activation of G-proteins (Gα, Gβ and Gγ), activating the PI3K, PLA2, TorC2 and sGC pathways in parallel. Each signaling network regulates cytoskeletal organization.

1.3 Excitable signaling

A PIP3-enriched domain on the cell membrane is transiently produced in an autonomous manner independent of the cytoskeleton [3]. In addition, it shows wave-like localization patterns in a typical environment [1], [15]. These domain formations spontaneously occur in the absence of extracellular stimuli, and the domain size is a few microns in diameter. Spontaneous activities of PIP3 are biased along the cAMP gradient, leading to a change from random to directional migration [45], [62].

PIP3 dynamics with the above features has been explained by so-called intrinsic excitable system (Fig. 1.2). An excitable system describes the dynamics of action potentials in neurons and has been mathematically analyzed by the Hodgkin-Huxley and FitzHugh-Nagumo models [17], [38]. Excitability has since been discovered in various biological processes including chemotactic responses as well as gene expression patterns [49]. An excitable system does not the strict definition but it shows an all-or-none response in general. Therefore, an excitable system is able to amplify small inputs, that is, supra-threshold. In fact, PIP3-enriched domains show a relatively constant signal strength to an input no matter how strong, while the domain size depends on the input strength [19], [37]. Thus, an excitable system interprets extracellular cAMP gradient as directional information and functions as an internal biochemical compass of motile cells [45], [62]. Human neutrophils also exhibit PIP3 excitability on the cell membrane, suggesting that excitability is a conserved system for eukaryotic chemotaxis [50].

Another feature of excitability is the refractory period. During this period, the system shows no or a small response even to a stimulus beyond the threshold. In case of a neuron cell, the refractory period is installed in a tiny compartment of the membrane, and therefore action potential is able to propagate unidirectionally. The PIP3 pathway shows a refractory period of 30~60 sec [19], [37], which is longer than the time scale at which cells respond to dynamic chemical gradients. It is unknown if other chemotactic pathways have this excitable property, giving ambiguity to the physiological meaning of the refractory period.

In general, an excitable system is composed of fast positive feedback and delayed negative feedback regulation (Fig. 1.2). The strength of positive

feedback determines the threshold and produces all-or-none response. Strong positive feedback regulation is enough that spontaneous activation is occurred by the fluctuation of system without stimulus [45]. On the other hand, the duration of negative feedback defines the refractory period. The response of excitable system including these regulations is independent of stimulus pattern: pulse and step stimuli induce the identical response [37].

Fig. 1.2

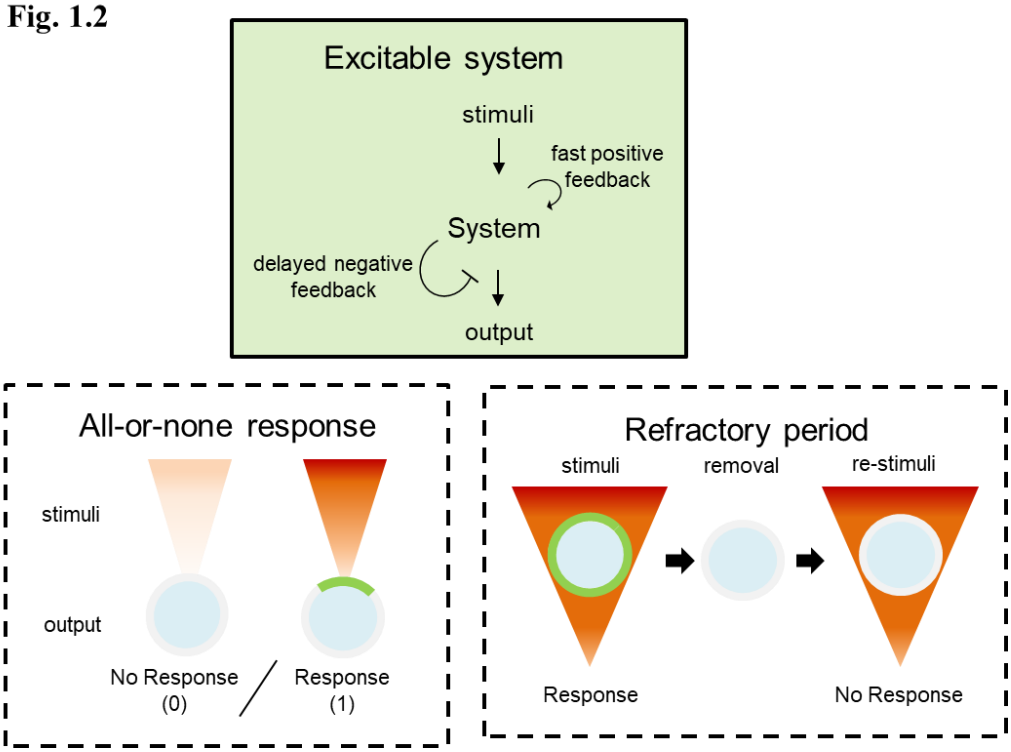

Fig. 1.2 A chemotactic excitable system.
The top column shows a simple model of an excitable system containing two feedback loops. The bottom column shows the features observed in an excitable system like the PIP3 pathway. The system exhibits a defined response to a supra-threshold stimulation (bottom left). Once the excitation starts, the system cannot respond to any stimuli (bottom right).

1.4 sGC and cGMP pathways

Among parallel pathways, the sGC pathway has been documented to contribute to the chemotaxis of *Dictyostelium* cells [59]. A series of mutant analyses revealed that the sGC pathway is important in chemotactic signaling (Fig. 1.3A) [28], [29]. One function of the sGC pathway is its enzymatic activity. Extracellular cAMP induces transient cGMP production in cells, which serves as a second messenger for posterior contraction via the regulation of myosin II [48]. cGMP is synthesized by two different guanylyl cyclases, cytosolic sGC and membrane-embedded guanylyl cyclase A (GCA) [39], [40]. The expression level of sGC becomes higher at the cell aggregation stage, therefore, sGC is the main supplier of cGMP.

Bioinformatic analysis has discovered four cGMP-binding candidate proteins, GbpA-D [16]. All four proteins have cyclic nucleotide binding motifs, but biochemical experiments have revealed that GbpC is a major cGMP effector [5]. Intracellular cGMP is degraded by two cGMP phosphodiesterases, GbpA and GbpB [5]. GbpA mainly contributes to the degradation of elevated cGMP, and GbpB is important for maintaining the basal cGMP level. On the other hand, GbpC and GbpD are signaling molecules relevant to physiological processes. GbpC has multiple domains consisting of leucine-rich repeats (LRR), Ras domain, Cor domain, MAPKKkinase domain and cGMP binding domain [52]. The intramolecular activation of GbpC induced by cGMP is required for myosin II regulation at the posterior side. GbpD regulates cell adhesion through its guanine nucleotide exchange factor (GEF) activity for Rap1, though it has no cGMP binding ability [6], [26].

In addition to cGMP production, it has been suggested that the sGC pathway has another function at the anterior side of the cell [56]. sGC proteins localize to pseudopods through their N terminus without the enzymatic domain during random and chemotactic migration (Fig. 1.3B). Extracellular cAMP stimuli induce transient sGC localization in a manner similar to PIP3 [57]. Cells lacking the N terminus of sGC exhibit impaired chemotaxis [7]. Moreover, loss of the C terminus domain results in the same phenotype as the N terminus, suggesting that the N and C termini of sGC are required for sGC localization and stabilization in pseudopods, respectively. These observations suggest that the sGC pathway also activates pseudopod formation via regulation of the cytoskeleton.

Fig. 1.3

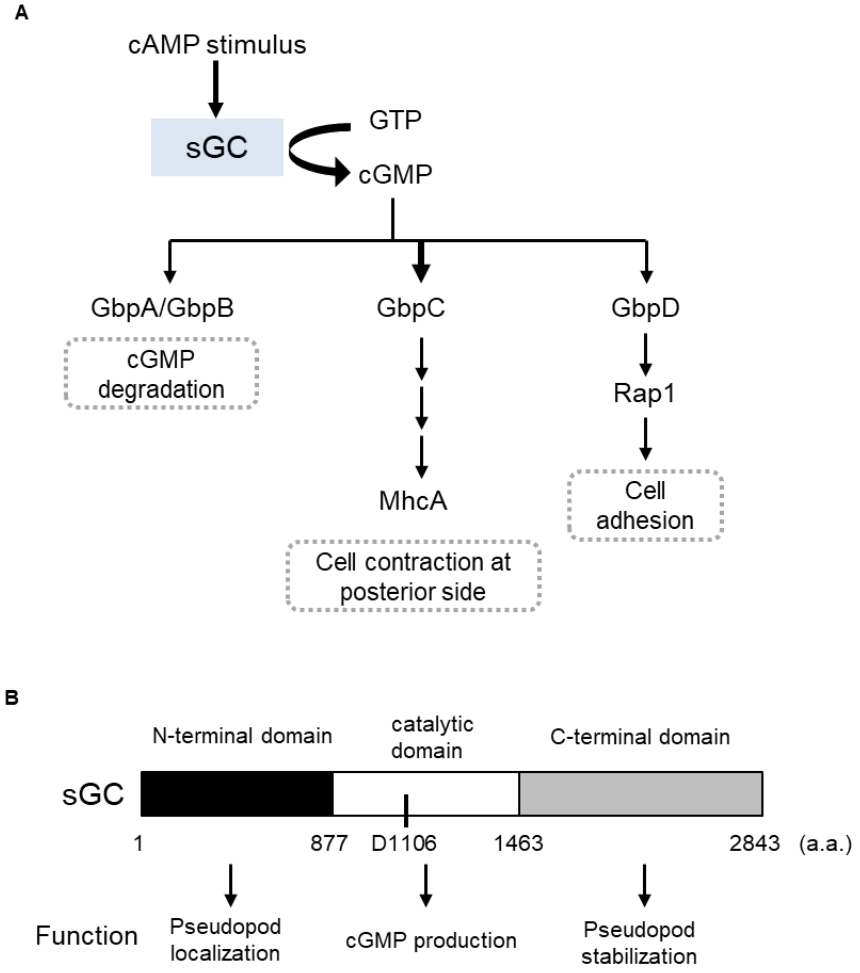

Fig. 1.3 sGC and cGMP signaling.
(A) cGMP signaling induced by a cAMP stimulus. cGMP produced by sGC activates GbpA-D. GbpA and GbpB are phosphodiesterases of cGMP. GbpC has MAPKKkinase function, which leads to myosin contraction at the posterior side. GbpD regulates cell adhesion through Rap1 activation.
(B) The domain structure of sGC. sGC is roughly divided into three domains: N-terminal, catalytic and C-terminal domains.

1.5 Results summary

To reveal the relationship between parallel pathways contributing to cell migration, I demonstrated that sGC localization shows excitable characteristics. Using pulse cAMP stimuli, I proved that sGC localization exhibits excitable behaviors including an all-or-none response, wave-like pattern formation and refractory period. Interestingly, the refractory period of sGC is shorter than that of PIP3, and the sGC pathway is suitable for rapid directional changes.

The observation of sGC localization in a series of cGMP signaling mutants revealed that sGC localization is negatively regulated by cGMP-GbpC signaling. Repeated responses by F-actin and sGC to pulse stimuli differed in these mutants, suggesting that sGC localization and F-actin are incorporated into one excitable network, the refractory period of which is determined by the cGMP level. In addition, purified sGC and F-actin exhibited co-localization and conformational changes in vitro. These results suggest that the sGC pathway regulates positive and negative feedback, which are important for deciding the excitable behavior.

Moreover, I simultaneously observed both sGC and PIP3 in a single cell. These excitable systems exhibited pseudopod localizations at different frequencies in individual cells. sGC localized to the pseudopod more frequently than PIP3, which is consistent with the short sGC refractory period. In fact, sGC was able to react to the positional changes of the chemoattractant source, while PIP3 could not.

Overall, these results illustrate that multiple signaling pathways regulate pseudopod dynamics differently through their characteristic excitable properties for chemotactic motility.

Chapter 2

Materials and Methods

2.1 Materials

2.1.1 Plasmids construction

Gene sequences were obtained from Dictybase (http://dictybase.org/), and PCR-amplified sequences were incorporated into vectors by Ligation (TOYOBO) or In-Fusion methods (TaKaRa). All plasmids are listed in Table 2.1. The N-terminal fragment (sGC_N, amino acids 1-1019) and N-terminal deletion fragment (sGCΔN, amino acids 877-2843) of sGC were amplified by PCR and cloned into pHK12-Halo7 to yield C-terminal Halo7 tagged proteins. The full-length *gbpA* gene was amplified by PCR and cloned into pDM358-eGFP to yield C-terminal eGFP tagged protein. To make *sgcΔ* cells, a gene disruption cassette containing blastcidin S resistance (BSR) gene was used. Two regions of the *sgc* sequence, amino acids 607 to 1116 and 4194 to 4891, were used, and the *BSR* gene was inserted between them. For protein purification, a series of sGC genes (sGC, sGC_N, and sGC_C (the C-terminal fragment: amino acids -2843)) were inserted into the PJK1-GFP-Flag vector.

Table 2.1 Plasmid list.

Plasmid name	Protein expressed	Tag	Backbone	Source or reference
Flag-Flag-GFP		Flag-Flag-GFP	pJK1	Kamimura et al., 2016
sGC-GFP	SgcA	GFP	pMB74	Veltman et al., 2005
sGC-GFP-Flag	SgcA	GFP-Flag	pJK1	this study
sGC_N-GFP-Flag	SgcA(1-1019)	GFP-Flag	pJK1	this study
sGC_C-GFP-Flag	SgcA(1463-2843)	GFP-Flag	pJK1	this study
sGCΔcat-GFP	SgcA(D1106A)	GFP	pMB74	Veltman et al., 2006
sGC_N-Halo7	SgcA(1-1019)	Halo7	pHK12	this study
sGCΔN-Halo7	SgcA(877-2843)	Halo7	pHK12	this study
PH_{PKB}-eGFP	PkbA(1-113)	eGFP	pBIG	Meili et al., 1999
mRFP-LimEΔcoil	LimE(1-145)	mRFP	pHK12	this study
GbpA-eGFP	GbpA	eGFP	pDM358	this study

Numbers in parentheses refer to a mutation or regions of amino acid residues.

2.1.2 Cell lines

Dictyostelium discoideum cells were grown at 22 ℃ in HL5 medium supplemented with 6 ng/ml Vitamin B12 and 100 ng/ml folic acid [60]. All cell strains are listed in Table 2.2. Wild-type AX2 and AX3 cells were used in this study. The AX2 cell line was used for simultaneous imaging of sGC_N-Halo7, PH_{PKB}-GFP, sGC-GFP and mRFP-LimEΔcoil. Because *pi3k1Δ2Δ* and *arcB* mutant cells were derived from the AX2 cell line, sGC-GFP responses in these strains were compared to AX2 cells. AX2 cells were also used for the protein purification of sGC-GFP-Flag (sGC-GFPF), sGC_N-GFP-Flag (sGC_N-GFPF) and sGC_C-GFP-Flag (sGC_C-GFPF) along with Flag-Flag-GFP (F_2GFP) as the control. AX3 cells were used as controls when observing sGC-GFP and mRFP-LimEΔcoil localization, because the mutant strains *gcΔ (sgcΔ/gcaΔ), gbpAΔ, gbpABΔ, gbpCΔ, gbpDΔ* and *mhcAΔ* were derived from the AX3 cell line. After gene transfer by electroporation, when cells were grown with selection, the medium was supplemented with 10 μg/ml blasticidin S, 20 μg/ml G-418 or 50 μg/ml hygromycin B. *sgcΔ* cells were generated from AX2 by homologous recombination using the gene disruption cassette described above. Electroporated cells were selected with 10 μg/ml blasticidin S. The cloned transformants were screened by PCR of their isolated genomic DNAs.

Table 2.2 Strain list.

Strain name	Genotype	Background	Source or reference
AX2		AX2	Lab stock
AX3		AX3	NBRP
sgcΔ	*sgcAΔ*	AX2	this study
gcΔ	*sgcAΔ, gcAΔ*	AX3	Veltman et al., 2006
pi3k1Δ/pi3k2Δ	*pikAΔ, pikBΔ*	AX2	Kamimura et al., 2016
gbpAΔ	*pdeDΔ*	AX3	Bosgraaf et al., 2002
gbpABΔ	*pdeDΔ, pdeEΔ*	AX3	Bosgraaf et al., 2002
gbpCΔ	*gbpCΔ*	AX3	Bosgraaf et al., 2002
gbpDΔ	*gbpDΔ*	AX3	Bosgraaf et al., 2002
mhcAΔ	*mhcAΔ*	AX3	Ruppel et al., 1994
abpACΔsevAΔ	*abpAΔ, abpCΔ, sevAΔ*	AX2	Shindl et al., 1992
arcB	arcB(I191L/D197Y/K206V/A213V/F223L/ P224S/ E232G/I237T/H245L/S250S)	AX2	Langridge and Kay, 2007
Flag-Flag-GFP/AX2		AX2	this study
sGC-GFP-Flag/AX2		AX2	this study
sGC_N-GFP-Flag/AX2		AX2	this study
sGC_C-GFP-Flag/AX2		AX2	this study
PH_{PKB}-eGFP/sGC_N-Halo7/AX2		AX2	this study
sGC-GFP/mRFP-LimEΔcoil/AX2		AX2	this study
sGC-GFP/AX2		AX2	this study
mRFP-LimEΔcoil/AX3		AX3	this study
sGCΔN-Halo7/*sgcΔ*	*sgcAΔ*	*sgcΔ*	this study
PH_{PKB}-eGFP/sGCΔN-Halo7/*sgcΔ*	*sgcAΔ*	*sgcΔ*	this study
sGC-GFP/*gcΔ*	*sgcAΔ, gcAΔ*	*gcΔ*	Sato et al., 2009
sGCΔcat-GFP/*gcΔ*	*sgcAΔ, gcAΔ*	*gcΔ*	Sato et al., 2009
mRFP-LimEΔcoil/*gcΔ*	*sgcAΔ, gcAΔ*	*gcΔ*	this study
sGC-GFP/*pi3k1Δ2Δ*	*pikAΔ, pikBΔ*	*pi3k1Δ/pi3k2Δ*	this study
sGC-GFP/*gbpAΔ*	*pdeDΔ*	*gbpAΔ*	this study
mRFP-LimEΔcoil/*gbpAΔ*	*pdeDΔ*	*gbpAΔ*	this study
mRFP-LimEΔcoil/GbpA-eGFP/*gbpAΔ*	*pdeDΔ*	*gbpAΔ*	this study
sGC-GFP/*gbpABΔ*	*pdeDΔ, pdeEΔ*	*gbpABΔ*	this study
sGC-GFP/*gbpCΔ*	*gbpCΔ*	*gbpCΔ*	this study
mRFP-LimEΔcoil/*gbpCΔ*	*gbpCΔ*	*gbpCΔ*	this study
GbpC/*gbpCΔ*	*gbpCΔ*	*gbpCΔ*	van Egmond et al., 2008
GbpCΔcGMP/*gbpCΔ*	*gbpCΔ*	*gbpCΔ*	van Egmond et al., 2008
GbpCΔkinase/*gbpCΔ*	*gbpCΔ*	*gbpCΔ*	van Egmond et al., 2008
sGC-GFP/*gbpDΔ*	*gbpDΔ*	*gbpDΔ*	this study
sGC-GFP/*mhcAΔ*	*mhcAΔ*	*mhcAΔ*	this study
sGC_N-Halo7/*abpACΔsevAΔ*	*abpAΔ, abpCΔ, sevAΔ*	*abpACΔsevAΔ*	this study
sGC-GFP/*arcB*	arcB(I191L/D197Y/K206V/A213V/F223L/ P224S/ E232G/I237T/H245L/S250S)	*arcB*	this study

NBRP, National BioResource Project in Japan.

2.2 Methods

2.2.1 Cell preparation for experiments

Cells for microscopic observation were starved for 5~7 h in development buffer consisting of 10 mM Na/KPO_4 (pH 6.5), 2 mM $MgSO_4$ and 0.2 mM $CaCl_2$. For cAMP stimulation experiments, cells were treated with 4 mM caffeine for 30 min to inhibit *de novo* adenylyl cyclase activity and deplete extracellular cAMP. Cells were placed on glass-bottom dishes (IWAKI) for the observation.

2.2.2 Fluorescence imaging and pulse cAMP stimulation

Fluorescence images were obtained by using a confocal microscope (FV1000, Olympus) with a 60×/1.35 NA oil immersion objective lens and software (Fluoview, Olympus). TMR and mRFP were excited by a 543 nm He-Ne laser, and GFP was excited by a 488 nm Ar laser. For pulse cAMP stimulation, cells were placed on a 4-cm round cover glass (Matsunami) with a flow chamber (FCS2, Bioptics). The inlet of the chamber was connected to a 10-ml glass syringe (Top) mounted in syringe pumps (FP-1000, Melquest). The syringe was filled with development buffer containing 4 mM caffeine and 5 nM DEACM–caged cAMP (Biolog). The photolytic activation of caged cAMP by a 405 nm mercury lamp was carried out upstream of the cells, and activated cAMP was flowed out (Fig. 2.1A). To demonstrate the temporal change of the cAMP concentration, 100 μM CMNB-caged fluorescein (Invitrogen) was used instead of caged cAMP (Fig. 2.1B). The flow rate was 300 μl/min. In repetitive stimulus experiments, all exposures were carried out by 1.5 sec laser irradiation. To align the first pulse timing, data were normalized by the maximum value of the cytosolic fluorescence intensity. In the case of repetitive stimuli by changing the first stimulus duration, data were acquired from the end of the first stimulus, and the cytosolic fluorescence intensity was normalized as above.

Fig. 2.1

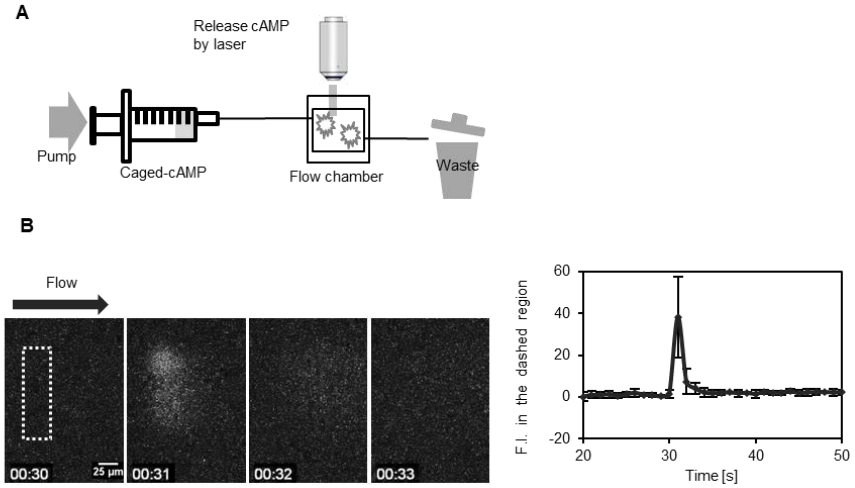

Fig. 2.1 Construction of the cAMP pulse stimulation system.
(A) A schematic drawing of the pulse stimulation system.
(B) Time course of the transient release of caged compound. Photolysis of 100 μM caged fluorescein in solution was carried out at the dashed region by UV flash (left). Fluorescence intensity (F.I.) of the region where UV was irradiated (right) (mean ± s.d. for n = 3). Time format is “”mm:ss”.

2.2.3 Pseudopod characterization and cell motility assay

Differentiated cells without caffeine treatment were put on a glass bottom dish and captured by the confocal microscope at 5 sec intervals for at least 5 min. The pseudopod dynamics was analyzed by ImageJ according to the localization patterns of sGC and PIP3 (Fig. 2.2). The positions of the sGC and PIP3 signals were assigned from the fluorescence images to distinguish two types of localization: sGC alone and the co-localization of sGC and PIP3. Morphological changes were extracted by differentiating between two consecutive binarized fluorescence images. In this study, I defined a pseudopod as an area that extended beyond 4 μm^2/frame during growth. These extracted pseudopods were characterized by quantifying the size, the appearance frequency, the lifetime, and the contribution to cell movement. The size was defined by the elongation length between the beginning and end points of a pseudopod during its total life cycle. The appearance frequency, or the average number of pseudopods per cell, was calculated by dividing the total number of pseudopods on each cell by the recorded time. The lifetime is the length of time in which a positive change was maintained in each pseudopod's area. The contribution to cell movement was defined as the displacement of the centroid of a pseudopod during its lifetime.

Fig. 2.2

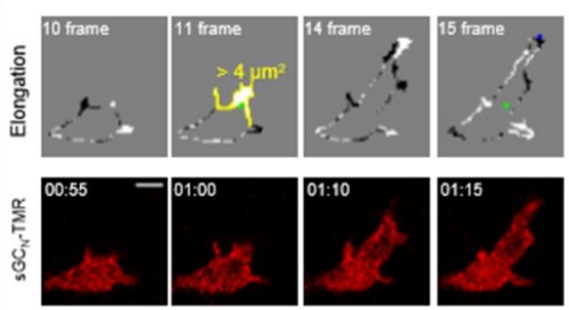

Fig. 2.2 A representative pseudopod analysis.
The fluorescence image of a cell with sGC_N-TMR shown in the bottom panels was binarized and subtracted in two consecutive frames. The white and black colors in the upper panel show the positive and negative changes, respectively. An area more than 4 μm^2 (shown by the yellow ROI) was defined as a pseudopod and was pursued when it stopped expanding. The green and blue dots show the start and end points of the pseudopod, respectively.

For cell motility analysis, developed cells without caffeine treatment were observed with an Olympus IX-71 inverted microscope capable of phase contrast optics. Movie files were recorded with a CCD camera (Digital Sight, Nikon) and software (NIS-Elements, Nikon). Cell behavior was recorded for 20 min at 5-sec intervals, and images were analyzed using laboratory-developed software. The motility speed of each cell was calculated as the average speed for each short trajectory.

2.2.4 sGC localization analysis on the cell surface

The localization of sGC-GFP to the cell surface was analyzed by ImageJ. The fluorescence intensity profile of sGC-GFP on the cell surface was obtained at every pixel along the cell periphery and processed with a 15-pixels moving average. In order to compensate for different sGC-GFP expression levels, profiles were normalized by the membrane fluorescence intensity in the absence of sGC localization. To compare sGC localization under various conditions, I defined localization amplitude and domain size as follows. Localization amplitude represents the maximum value of the normalized intensity along the cell membrane. Domain size was quantified as the ratio of the region with the normalized value exceeding the threshold to the overall membrane area. The threshold was set as 1.2 in this report.

2.2.5 Kymograph analysis

The spatiotemporal dynamics of fluorescence probes on the cell membrane was analyzed and shown as 2D patterns by ImageJ. To monitor the pseudopod dynamics of moving cells, kymographs of the mRFP-LimEΔcoil localization in Fig. 3.12B were generated using an ImageJ plugin. The second response time was defined as the time that a cell showed mRFP-LimEΔcoil localization after its first response to 10 nM cAMP. Some cell lines showed a persistent response without transient suppression. The second response time of those cells was counted as 0. sGC_N-TMR and PH_{PKB}-GFP localizations on the bottom surface of the cell in Fig. 3.16 were analyzed by the reslice function in ImageJ after 1.0-pixel mean filtering of the movie.

2.2.6 Cytoskeletal actin assay

As previously described [24], differentiated cells were incubated in phosphate magnesium buffer (2 mM $MgSO_4$ in 5 mM Na/KPO_4 buffer, pH 6.5) with 3 mM caffeine at 3×10^7 cells/ml. The cell suspension was stimulated with cAMP at a final concentration of 10 nM. After stimulation, the cells were lysed by adding equal volumes of 2× assay buffer consisting of 2% Triton X-100, 20 mM KCl, 20 mM EGTA, 20 mM imidazole and 0.1 mg/ml NaN_3, and incubated on ice for 10 min. The samples were centrifuged at 8,000 ×g for 4 min to collect the pellet fraction followed by washing with 1× assay buffer and boiled in 2× SDS sample buffer. Finally, the samples were analyzed by PAGE and stained with Coomassie Brilliant Blue. Images were acquired with ImageQuant LAS4000 for the quantification of actin (40 kDa).

2.2.7 Preparation of F-actin

The purification of actin was carried out by using rabbit muscle acetone powder (Sigma-Aldrich). The purification method was referred to the protocols at Ostap Laboratory (https://www.med.upenn.edu/ostaplab/protocols-and-software.html) and Dictybase (http://dictybase.org/). Dissolved actin in buffer A (0.2 mM ATP, 0.5 mM DTT and 0.2 mM $CaCl_2$ in 2 mM Tris-Hcl buffer, pH 8.0) was polymerized by adding 50 mM KCl and 2 mM $MgCl_2$. F-actin was collected by ultracentrifugation and depolymerized by dissolving in buffer A. Finally, actin protein was dialyzed for 3 days. The concentration of purified actin was measured by reading O.D. 290 and diluted to 2 mg/ml. Finally, 2 mg sucrose/mg actin was added to the stock, which was then stored at -80 ℃ until use. Actin was polymerized in buffer F (buffer A in 500 mM KCl, 10 mM ATP and 20 mM $MgCl_2$) at room temperature for 1 h.

For microscopic observations, F-actin was stabilized by adding 6.6 μM Rhodamine-Phalloidin (Rh-Ph, Molecular Probes)/6.25 μM F-actin. Purified proteins and Rh-Ph labeled F-actin were mixed in 0.1% Triton-X added buffer F at room temperature for 20 min. Fluorescence observations were carried out on EtOH-washed slide glasses.

2.2.8 Protein purification

GFP-Flag-tagged sGC (sGC-GFPF), sGC_N (sGC_N-GFPF), sGC_C (sGC_C-GFPF)

and control Flag-Flag-GFP (F_2GFP) proteins were purified from *Dictyostelium discoideum* cells [24]. Cells expressing each protein were starved for 1 h and lysed on ice in CHAPS lysis buffer consisting of 40 mM Hepes (pH 7.5), 120 mM NaCl, 20 mM NaF, 2 mM Na_3VO_4, 20 mM sodium pyrophosphate, 0.3% CHAPS and complete EDTA-free protease inhibitor (Roche) for 5 min followed by centrifugation for 15 min to remove debris. WCEs were pretreated with Sepharose 4B beads for 30 min, and unbound supernatant was incubated with anti-Flag M2 beads (Sigma-Aldrich) at 4 ℃ for 2 h. Protein samples were eluted with Flag peptide in CHAPS lysis buffer following extensive washing.

Chapter 3

Results

3.1 The sGC pathway is an excitable system

3.1.1 Excitability of sGC localization

In order to investigate the relationship between parallel pathways, I determined whether sGC localization shows the excitable features seen with PIP3. If the sGC pathway is also an excitable system, then sGC localization should exhibit excitable behaviors such as an all-or-none response, wave-like propagation and a refractory period. These dynamics are caused by an intrinsic excitable mechanism. I assumed that a cAMP pulse stimulus with a very short duration would induce the same response in sGC localization as a cAMP stepwise stimulus. For this purpose, I used an experimental system composed of caged-cAMP and a flow chamber. Cells do not respond to caged-cAMP itself, and uncaging by light irradiation produces cAMP around the cells. The combination of caged-cAMP and flow chamber allows us to control the timing and strength of the cAMP stimuli by manipulating the exposure times of the UV irradiation (see Methods and Fig. 2.1A). Upon UV flash at the upstream region of the cells, cAMP was applied to and removed from the cells within a few seconds by the flow (Fig. 2.1B). This time length is short enough to test the excitability of sGC, because sGC localizes around 10 sec and returns to resting state around 30 sec after the stimulus [56].

I used the cell line in which the C-terminal fusion of GFP to full-length sGC (sGC-GFP) was expressed in *gcΔ* (*sgcΔ/gcaΔ*) cells. Cytosolic sGC-GFP exhibited translocation to the cell surface transiently in response to a pulse stimulus within 2 sec of UV exposure as well as a step stimulus of 100 nM cAMP (Fig. 3.1A). The two transient responses had the same temporal changes and same strength. The sGC localization dynamics transmitted these different signals to the same responses, indicating that the response is produced intrinsically by the system itself in a manner independent of the stimulus pattern. Furthermore, I examined the dose-dependent response of sGC localization by changing the UV exposure times. sGC-enriched domain was generated in the absence of cAMP (shown by Sp in Fig. 3.1B) and by UV irradiation. Quantitative analysis (see Methods) revealed that the sGC domain size on the cell surface expanded with increasing UV irradiation time. On the other hand, the domain amplitudes remained relatively constant (Fig. 3.1B). I also uniformly stimulated the cells with defined cAMP concentrations and observed the sGC-GFP responses (Fig. 3.1C). Similar to Fig. 3.1C, the domain size on the cell surface increased up to ~60% of the cell surface until 0.1 nM cAMP with constant domain amplitude. Additionally, spontaneous sGC localization without external stimuli showed a similar domain size with the same amplitude in the restricted region of the cell surface. These results reflect how sGC localization follows all-or-none laws like that observed in PIP3 excitation previously [37].

Fig. 3.1

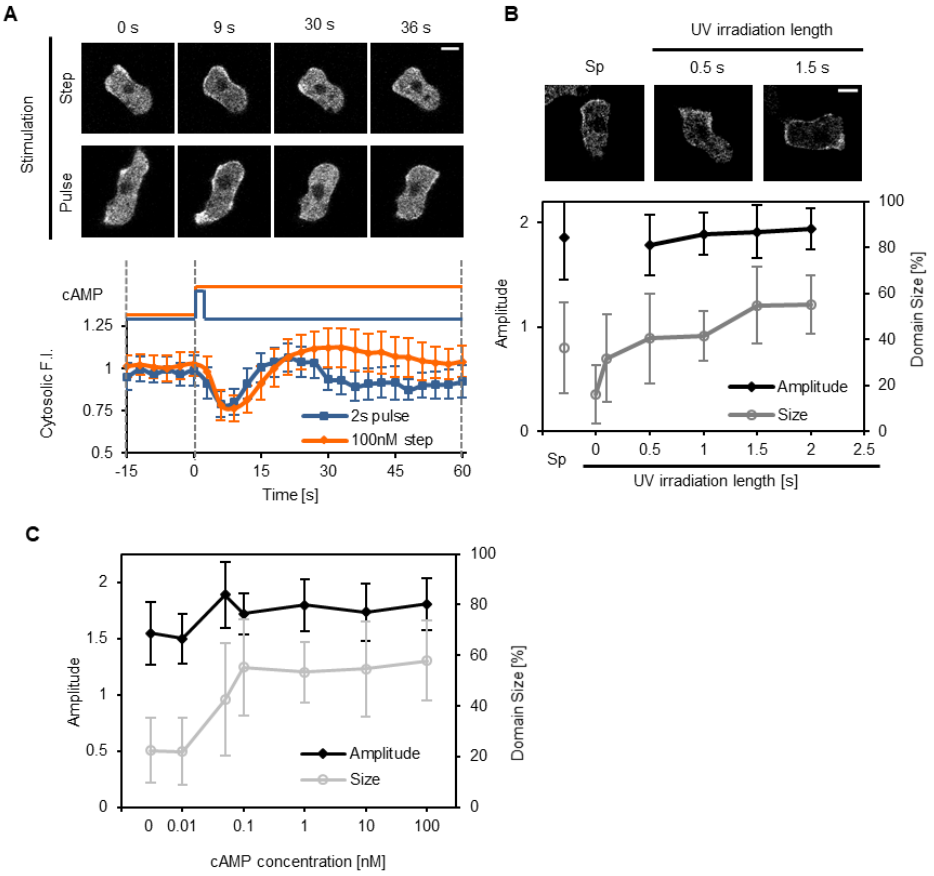

Fig. 3.1 Excitable dynamics of sGC localization at the membrane.
(A) A *gcΔ* cell expressing sGC–GFP was stimulated upon pulse and step inputs of cAMP. Representative images after a 100 nM step (top row) or 2 s pulse (bottom row) stimulus are shown. The bottom panel shows the comparison between sGC–GFP responses to pulse (blue) and step (orange) inputs. Responses (mean ± s.d. for n=12 and 24 cells, respectively) of cytosolic sGC–GFP fluorescence intensity (F.I.) were normalized to the pre-stimulus level.
(B) Excitable features of sGC–GFP localization were assessed by using UV-sensitive caged cAMP (see Materials and Methods). A *gcΔ* cell expressing sGC–GFP was stimulated via various UV exposure times (top). The response amplitude and domain size of the sGC-enriched region are shown as functions of UV exposure time (bottom). Characteristics of the spontaneously formed domain are shown as Sp (mean ± s.d. for at least 17 cells).
(C) *gcΔ* cells expressing sGC-GFP were stimulated with various cAMP concentrations. Response amplitude and domain size of the sGC-enriched region are shown as functions of the cAMP concentration (mean ± s.d. for at least 8 cells). Scale bars: 5 μm.

Next I determined whether sGC localization at the cell surface exhibits a refractory period by repeated pulse stimuli. If sGC localization has a refractory period, it would exhibit no or a small response to the second and third stimuli separated by a very short interval. *gcΔ* cells expressing full length sGC-GFP were stimulated repeatedly at different time intervals (Fig. 3.2A, B). At 21-sec and 30-sec intervals, sGC-GFP responded identically to all stimuli. However, in response to repetitive stimuli at 12-sec intervals, the first response was normal, but the second and third responses were progressively weaker. These results indicate that the sGC localization has a refractory period between 10-20 sec, which is shorter than that of PIP3 reported previously (30-60 sec).

Fig. 3.2

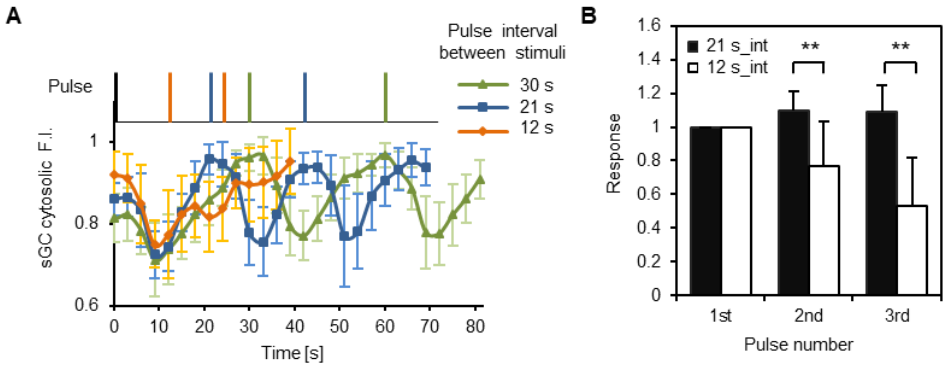

Fig. 3.2 The refractoriness of sGC-GFP localization at the membrane.
(A) A *gcΔ* cell expressing sGC–GFP was stimulated with 1.5 s pulsatile UV exposure three times. Cytosolic sGC–GFP responses to stimuli of various interval lengths were normalized to the maximum fluorescence value (F.I.) in the time course. Black and color-coded bars show the first stimulus timing and the pulse timing at different interval lengths, respectively.
(B) Each cytosolic response in (A) was normalized to the value of the first response (mean + s.d. for at least 13 cells). **P<0.001 (t-test).

Another feature of an excitable system is wave-like propagation [25], [41], which is often observed when the excitable parameters are modulated. In *Dictyostelium* cells, when cells are treated by a certain concentration of latrunculin A (LatA), an actin polymerization inhibitor, PIP3 and F-actin localization on the cell surface show typical examples of traveling wave generation [1], [14]. When I mildly perturbed the actin cytoskeleton with a low concentration of LatA, F-actin showed wave-like propagation on the bottom surface of the cells, as visualized by the fluorescent F-actin probe mRFP-LimEΔcoil (Fig. 3.3A) [13]. sGC-GFP and mRFP-LimEΔcoil exhibited co-localization and propagation on the cell surface. In contrast, PIP3 and F-actin exist side by side [15]. Furthermore, cAMP-induced sGC localization at the cell surface was significantly reduced in mutant cells lacking functional ArcB, a subunit of the Arp2/3 complex, which is responsible for actin polymerization (Fig. 3.3B) [30]. These results imply that the excitable behavior of sGC relies on F-actin activity. Overall, the existence of the all-or-none response, refractory period and propagating waves proves the excitability of the sGC signaling pathway.

Fig. 3.3

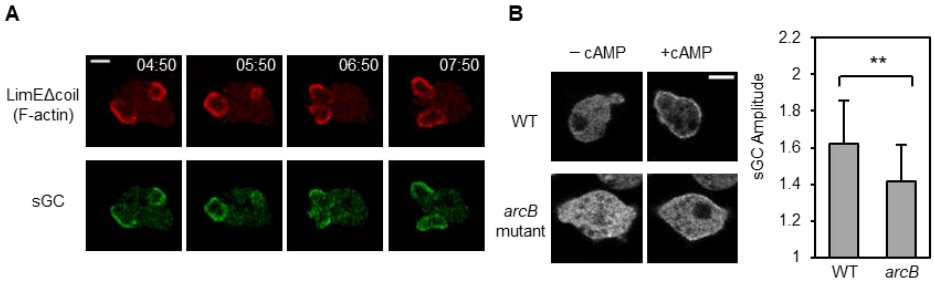

Fig. 3.3 sGC localization depends on the existence of F-actin.
(A) Co-localization pattern of F-actin and sGC. A wild-type AX2 cell co-expressing mRFP–LimEΔcoil and sGC–GFP was treated with 1 μM LatA. The bottom of the cell was observed at 5-s intervals. Time format is mm:ss.
(B) Wild-type AX2 and arcB mutant cells expressing sGC–GFP were stimulated with 100 nM cAMP. Localization amplitude (mean + s.d. for n=24 and 23 cells, respectively) was quantified as in Fig. 3.1. **P<0.001 (t-test). Scale bars: 5 μm.

3.1.2 Parameter differences among excitable pathways

An excitable system has two important parameters that determine the responsiveness to stimuli: the threshold and the refractory period. To investigate the differences of these parameters between the sGC and PIP3 pathways, I simultaneously observed their excitable behaviors in individual cells. For the observation of sGC localization, I used Halo7-tagged protein as a sGC probe (sGC_N-Halo7), since sGC localizes to pseudopods through its N-terminal region. sGC_N-Halo7 was stained by tetramethylrhodamine (TMR) for multicolor imaging. Regarding PIP3, I used a previously reported PIP3 probe, the GFP tagged pleckstrin homology domain of *Dictyostelium* PKBA (PH_{PKB}-GFP) [3], [34], [57]. First, I compared the dose-responses by using stepwise cAMP stimuli to survey the threshold (Fig. 3.4A). The cytosolic fluorescence intensity of sGC and PIP3 exhibited no response, a relatively strong response and a saturated response to 0.1 nM, 0.3 nM and 10 nM cAMP, respectively. The gradual increase of the response between 0.3 and 10 nM reflects the increase of the domain size and the difference of the threshold in each cell. Thus, sGC and PIP3 almost identically responded to 0.3 nM cAMP, which indicates that the thresholds of sGC and PIP3 are comparable. I next observed these signaling molecules in cells lacking one of them (Fig. 3.4B, C). PIP3 localization was not dependent on sGC localization (Fig. 3.4B), and sGC showed a normal response despite little PIP3 (Fig. 3.4C). These results indicate that the localization thresholds of sGC and PIP3 are independent and regulated by a common signaling components.

Fig. 3.4

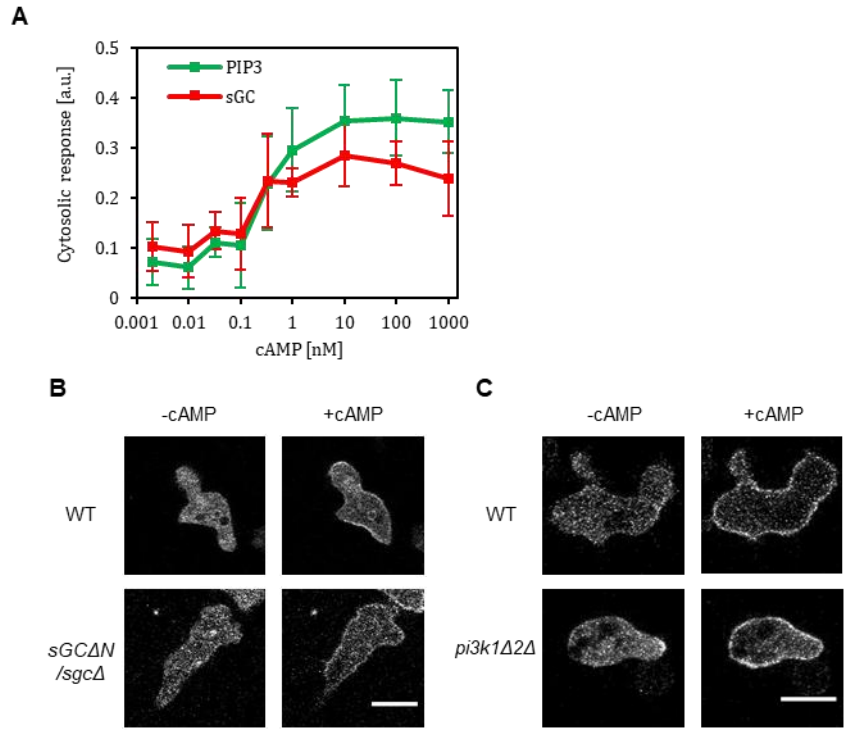

Fig. 3.4 Different response thresholds between PIP3 and sGC.
(A) Dose-responses of PH_{PKB}–GFP and sGC_N–TMR expressed in a wild-type AX2 cell were induced by stepwise cAMP stimuli. Each cytosolic fluorescence change was normalized to the pre-stimulus level (mean ± s.d. for n=13~18 cells).
(B, C) PIP3 and sGC responses of the indicated cell lines at 1 μM cAMP. PIP3 production by wild-type AX2 and sGCΔN/*sgcΔ* cells (B) and sGC localization on wild type AX2 and *pi3k1Δ2Δ* cells (C) were observed by the expression of PH_{PKB}-GFP and sGC-GFP, respectively. Scale bars: 10 μm.

Next I evaluated their refractory periods by using pulse cAMP stimuli (Fig. 3.5A). When stimulated repeatedly by UV irradiation at 21-sec intervals, sGC localization exhibited a response repeatedly to all stimuli, whereas PIP3 did not (Fig. 3.5A). At 60-sec intervals, sGC and PIP3 were able to respond to all stimuli (Fig. 3.5B). The refractory period of PIP3 localization was about 30-60 sec, consistent with previous reports [19], [37]. The result that sGC and PIP3 localizations are independent (Fig. 3.4B, C) suggests that their refractory periods also are unique. In fact, sGC localized to the cell surface in mutant cells lacking *pi3k1* and *pi3k2* genes upon repeated stimuli with a refractory period of 30 sec, indicating that sGC responsiveness to cAMP stimulation is independent of PIP3 production (Fig. 3.5C). Thus, the excitable dynamics of sGC has a unique refractory period that is shorter than that of PIP3. Therefore, the sGC pathway can respond to stimuli of short intervals (about 10-20 sec), but the PI3K-PTEN pathway cannot. These results indicate that cell has multiple compasses with different time scales.

Fig. 3.5

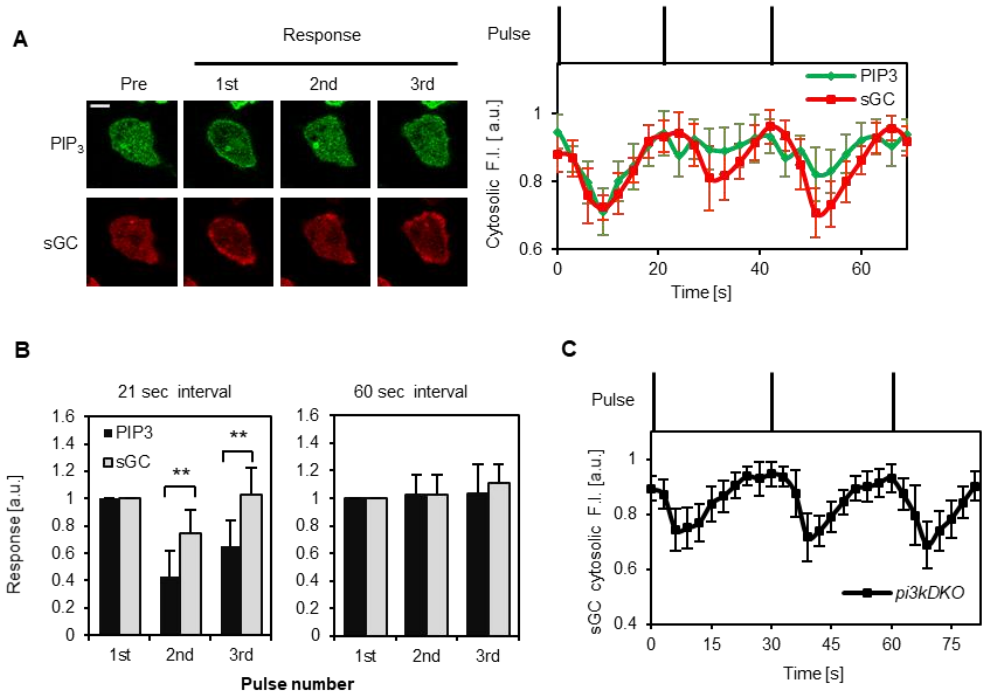

Fig. 3.5 Different refractory periods between PIP3 and sGC.
(A, B) A wild-type AX2 cell co-expressing PH_{PKB}–GFP and sGC_N–TMR was stimulated at 21-s or 60-s intervals by repetitive pulses. (A) Cytosolic responses to 21-s interval stimuli were normalized to the maximum fluorescence value (F.I.) in the time course. (B) Refractory responses of PH_{PKB}–GFP and sGC_N–TMR. Each cytosolic response to 21- or 60-s interval stimuli was normalized to the value of the first response (mean + s.d. for n=12 and 10 cells, respectively).
(C) sGC–GFP responses to 30-s interval stimuli in *pi3k1Δ2Δ* cells (mean ± s.d. for n=16 cells). Black vertical bars at the top in (A) and (C) represent the pulse timing. **P<0.001 (t-test). Scale bar: 5 μm.

3.2 Molecular mechanisms of sGC excitability

3.2.1 cGMP-GbpC signaling suppresses sGC and F-actin localization

In order to understand the excitable behavior of the sGC pathway, biochemical and mathematical molecular insights are important. An excitable system requires fast positive feedback to amplify the signal and delayed negative regulation to suppress it, resulting in transient excitation [9]. In the case of PIP3, cells lacking PTEN (*pten⊿*), the phosphatase of PIP3, show a prolonged response to stepwise cAMP stimuli [21]. This result indicates that PTEN is the main negative regulator of PIP3 excitability. sGC pathway has two functions: pseudopod formation through sGC localization, and pseudopod retraction by cGMP and its binding protein GbpC [5], [52]. These reports suggest the possibility that cGMP and GbpC are the negative feedback regulators for sGC localization.

To explore the molecular mechanisms of sGC excitability, I focused on the pathway's product, cGMP, and downstream signaling molecules, GbpA-D. To reveal the effect of cGMP on sGC localization at the cell surface, I first observed the cAMP-elicited responses of mutant sGC with a substituted amino acid (Asp1106Ala), which lacks catalytic activity (sGCΔcat). Tagged protein with GFP (sGCΔcat-GFP) was expressed in *gc⊿* cells [43], [56]. It was reported that *gc⊿* cells expressing sGCΔcat upon cAMP stimulation fail to produce cGMP [57].

Wild-type sGC-GFP exhibited translocation to the cell surface transiently upon cAMP stimulation and returned to the cytosol within 20 sec (Fig. 3.6A). On the other hand, the catalytically dead mutant sGCΔcat-GFP showed prolonged and stronger localization for several minutes as well as a PIP3 response in *pten⊿* cells, indicating that intracellular cGMP accelerates the dissociation of sGC from the cell surface. As a control, I examined the response of sGCΔcat-GFP in wild-type cells (Fig. 3.6B). sGCΔcat-GFP showed translocation to the cell surface upon cAMP stimulation in a similar manner to sGC-GFP. However, there were some differences in the behavior between sGC-GFP and sGCΔcat-GFP after 30 sec of stimulation: much more sGC-GFP returned to the cytosol than sGCΔcat-GFP. This effect is probably because the overexpression of sGC-GFP increases the cGMP level much more compared to that of wild-type cells [56]. I also examined the cAMP-mediated responses of wild-type and *gc⊿* cells, in which the C-terminal catalytic domain was deleted (sGC_N-GFP; Fig. 3.6C). As expected from the data of Fig. 3.6A, sGC_N-GFP translocated to the cell surface within 10 sec in both cells, but the returning phase to the cytosol was slower in *gc⊿* cells. Also, much more sGC-GFP dissociated from the cell surface in wild-type cells than sGC_N-GFP (compare Fig. 3.6B and 3.6C). When co-expressed in the same wild-type cells, sGC and sGC_N revealed almost the same dynamics upon cAMP stimulation, reaching equivalent cytosolic levels (Fig. 3.6D). These results further implicate intracellular cGMP in the dissociation of sGC.

Fig. 3.6

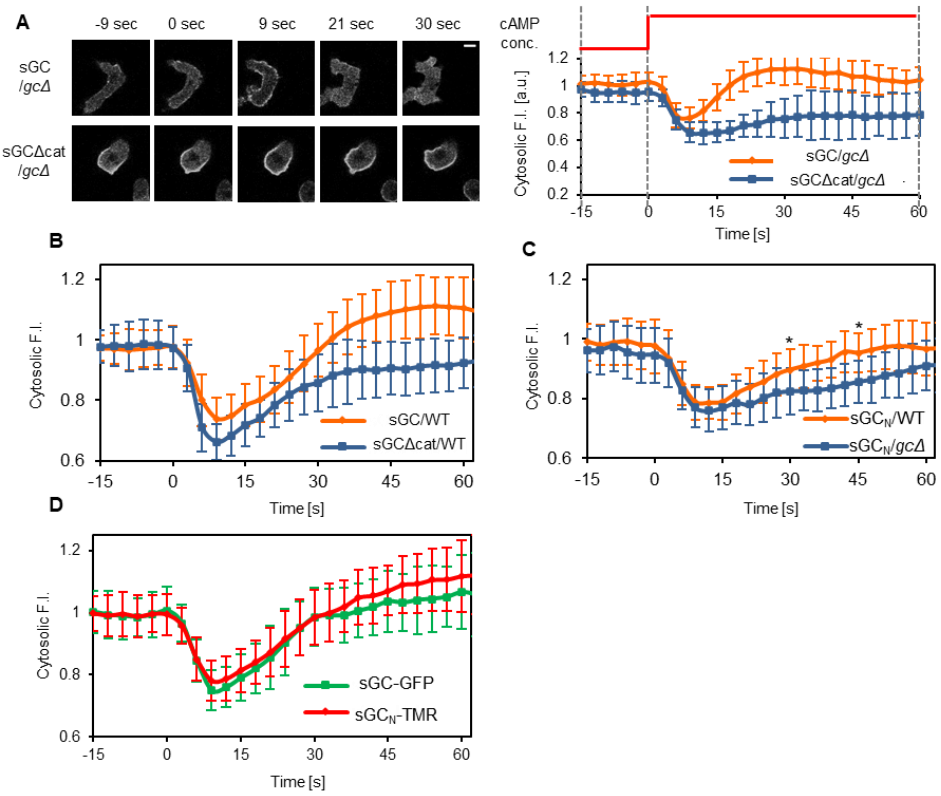

Fig. 3.6 sGC localization on the cell surface is sensitive to cGMP.
(A) *gcΔ* cells expressing sGC–GFP or sGCΔcat–GFP were stimulated with 100 nM cAMP. Representative images after the cAMP stimulus are shown. The time courses of the cytosolic fluorescence intensity of sGC (the same data is shown in Fig. 3.1A) and sGCΔcat are shown to the right (mean ± s.d. for n=24 and 17 cells, respectively). The red line shows the cAMP stimulation time. Scale bar: 5 µm.
(B) sGC responses of the indicated cell lines upon cAMP stimulation. Wild-type AX3 cells expressing sGC-GFP or sGCΔcat-GFP were stimulated with 100 nM cAMP. The cytosolic fluorescence intensity (F.I.) was normalized to the pre-stimulus level (mean ± s.d. for at least n = 19 cells).
(C) The responses of the sGC N terminus (sGC$_N$) in wild-type or *gcΔ* cells were observed (mean ± s.d. for n = 29 and 28 cells, respectively; * $P < 0.01$ versus wild-type cells at 30 and 45 sec, t-test).
(D) The responses of sGC and sGC$_N$ in the same wild-type cell were observed (mean ± s.d. for n = 19 cells).

Next I observed wild type sGC localization in a series of mutant cells lacking downstream signaling proteins GbpA and GbpB (*gbpABΔ*), GbpC (*gbpCΔ*) or GbpD (*gbpDΔ*). Among them, only *gbpCΔ* cells exhibited defects in sGC-GFP localization, in which sGC-GFP continued to localize on the cell surface stably in a manner similar to sGCΔcat-GFP (Fig. 3.7A). The other mutants exhibited no obvious changes in their localization at resting state without cAMP stimulation (Fig. 3.7A). When stimulated with cAMP, *gbpCΔ* cells exhibited prolonged responses in sGC-GFP translocation to the cell surface regardless of normal cGMP production (Fig. 3.7B). Thus, sGC localization at the cell surface is negatively regulated by its product, cGMP, and downstream signaling molecule, GbpC. This regulation ensures the transient response of sGC localization upon cAMP stimulation. In addition, *mhcAΔ* cells lacking myosin heavy chain exhibited transient responses of sGC localization on the cell surface upon cAMP stimulation, although the activity was less efficient than in wild-type cells (Fig. 3.7B). These results demonstrate that cGMP-dependent GbpC signaling regulates negatively the lifetime of sGC accumulation at the anterior side of the cell.

Fig. 3.7

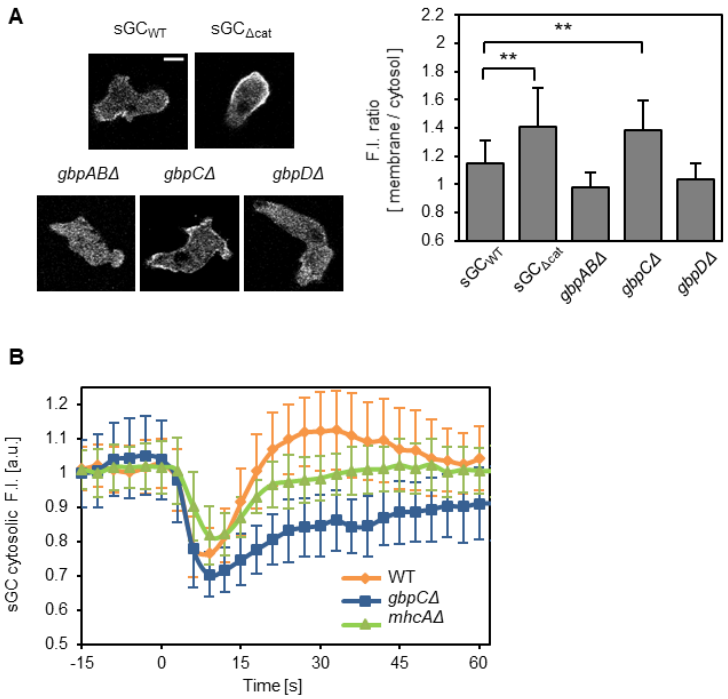

Fig. 3.7 cGMP-GbpC signaling suppresses sGC localization upon cAMP stimulation.
(A) Pseudopod sGC localization in the indicated knockout cell lines (left). The fluorescence intensity (F.I.) ratio (mean + s.d. for at least 25 cells) between the plasma membrane and the cytosol in the absence of cAMP (right). **P<0.001 (t-test). Scale bar: 5 µm.
(B) sGC responses of the indicated cell lines upon cAMP stimulation. Wild-type AX3 and mutant cells expressing sGC-GFP were stimulated with 100 nM cAMP. Cytosolic intensity was normalized to the pre-stimulus level (mean ± s.d. for at least n=19 cells).

Fig. 3.3 shows that sGC localization on the cell surface depends on F-actin, consistent with a previous report [56]. To examine the effects of cGMP-dependent GbpC signaling on F-actin polymerization in response to cAMP stimulation, I observed mRFP-LimEΔcoil in *gbpcΔ* cells (Fig. 3.8A). As the result, enhanced F-actin polymerization was observed as well as sGC localization (Fig. 3.7B). This persistent F-actin formation in *gbpCΔ* cells was also observed in a biochemical assay (Fig. 3.8B). GbpC has Ras-like Roc, RasGEF, and MAPKKkinase domains plus a cGMP-binding domain. It has been reported that cGMP binding to GbpC triggers intramolecular signal transduction, ultimately leading to kinase activation for myosin II contraction [52]. Therefore, I analyzed the involvement of this intramolecular signaling in GbpC-mediated F-actin response using deletion mutants of the MAPKKkinase or cGMP-binding domain. I found neither mutant was able to rescue the phenotype of excessive F-actin formation upon cAMP stimulation (Fig. 3.8B), suggesting that GbpC requires kinase activation following cGMP binding for the suppression of F-actin. On the other hand, *mhcAΔ* cells showed a transient F-actin response to cAMP stimulation as well as wild type cells (Fig. 3.8A). These results indicate that cGMP-dependent GbpC signaling functions to suppress sGC localization via F-actin regulation at the anterior side but not to contract myosin at the posterior side.

Fig. 3.8

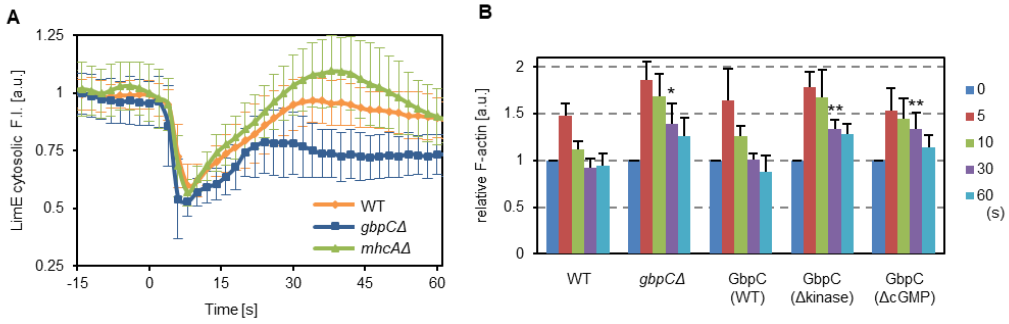

Fig. 3.8 cGMP-GbpC signaling suppresses F-actin polymerization.
(A) The indicated cell lines expressing mRFP–LimEΔcoil were stimulated by 10 nM cAMP. Cytosolic fluorescence intensity (F.I.) was normalized to the pre-stimulus level (mean ± s.d. for at least n=19 cells).
(B) Cytoskeletal F-actin quantities at 10 nM cAMP were normalized to the pre-stimulus level. GbpC (WT), GbpC (Δkinase) and GbpC (ΔcGMP) represent gbpCΔ cells expressing wild-type, kinase-dead and cGMP-binding mutants of GbpC, respectively (mean + s.d. for at least three experiments; *P<0.05 versus wild-type, **P<0.05 versus GbpC (WT) at 30 s, t-test).

3.2.2 cGMP levels regulate the refractory period

The above results suggest that cGMP-dependent GbpC signaling suppresses sGC localization at the cell surface and that this negative regulation recovers sGC excitation to the basal state. Therefore, cGMP and GbpC are important for determining the refractory period length. I observed sGC-GFP in *gbpCΔ* cells for evaluating the refractory period. Cells showed prolonged sGC-GFP responses to 12-sec and 21-sec interval stimuli (Fig. 3.9A), which resembles the response to step stimuli (Fig. 3.7B). These responses indicate that cells require GbpC to distinguish repeated pulse stimuli from continuous stimuli. Moreover, sGC-GFP in *gbpCΔ* cells responded to repetitive pulse stimuli at 30-sec intervals in a manner similar to sGC-GFP in wild-type cells (Fig. 3.2). Thus, I can conclude that sGC excitation can recover to the basal state within 30 sec because extracellular stimuli were completely removed. Next I observed sGC-GFP responses in a *gbpAΔ* cell line, in which the cGMP-specific phosphodiesterase gene is deleted. Because *gbpAΔ* cells are reported to show prolonged over-production of cGMP upon cAMP stimulation [32], it is expected that the refractory period become longer in *gbpAΔ* cells. *gbpAΔ* cells showed severely suppressed sGC-GFP responses to repeated stimuli at 21-sec intervals, while wild-type cells responded normally (Fig. 3.2 and 3.9B). This result suggests that persistent cGMP overproduction prolonged the refractory period for sGC localization. Thus, cGMP-dependent GbpC signaling is required for shortening the refractory period and provides a mechanism for the fast recovery of the sGC excitation in order to respond to the subsequent cAMP stimulation.

To further confirm these results, I observed whether the refractory period of F-actin depends on the cGMP level. *gbpAΔ* cells significantly reduced the second response to a 21-sec interval stimulus, while wild-type and rescued *gbpAΔ* cells revealed almost the same response to the first and second stimuli (Fig. 3.10A, B). These results suggest that the cGMP level is an important factor for determining the refractory period of sGC and PIP3.

Fig. 3.9

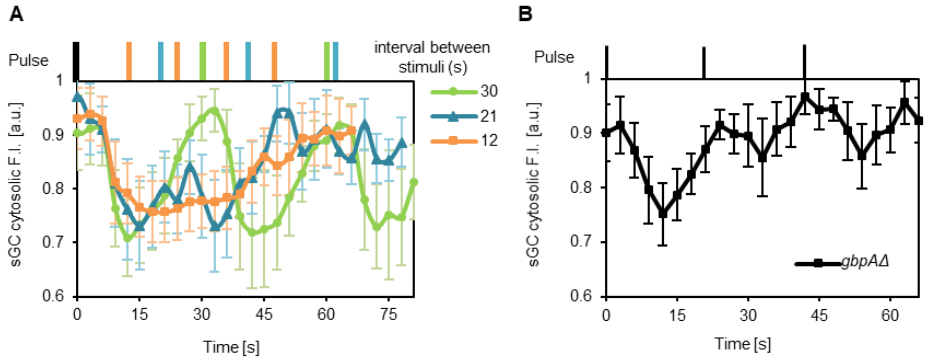

Fig. 3.9 cGMP–GbpC signaling regulates the refractoriness of sGC responses.
(A) Cytosolic sGC–GFP responses in *gbpCΔ* cells upon repetitive stimuli. Color-coded bars represent the pulse timing as shown in Fig. 3.2 (mean ± s.d. for at least 11 cells).
(B) The refractoriness of the sGC–GFP response depends on the amount of intracellular cGMP. *gbpAΔ* cells were repetitively stimulated with 21-s interval pulses (mean ± s.d. for n=16 cells).

Fig. 3.10

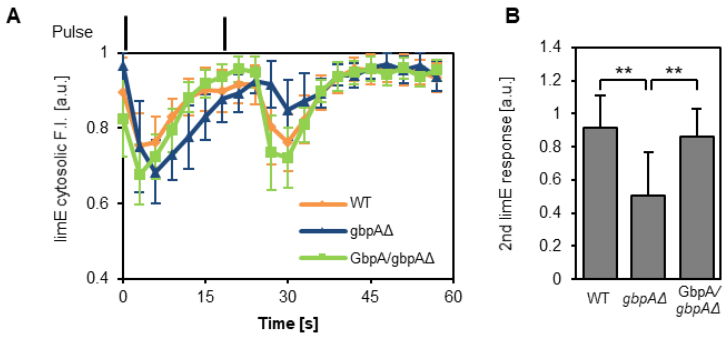

Fig. 3.10 GbpA, a phosphodiesterase of intracellular cGMP, plays an important role in the regulation of the F-actin response.
(A) The refractoriness of F-actin depends on the amount of intracellular cGMP. Wild-type AX3, *gbpAΔ* and *gbpAΔ* rescued by GbpA cells expressing mRFP-LimEΔcoil were repetitively stimulated with 21-s interval pulses (mean ± s.d. for n = 23 cells). Cytosolic responses to 21-s interval stimuli were normalized by the maximum fluorescence value (F.I.) in the time course. Black bars on the abscissa represent the pulse timing.
(B) The second responses were normalized by the first responses for each cell line (mean + s.d.; ** $P < 0.001$, t-test).

Intracellular cGMP production is dependent on cAMP concentration of stimulus [54]. Low concentration of cAMP stimulus induces cGMP production with relatively small peak and short duration. Therefore, I examined whether the refractory period depends on the stimulus pattern by changing the UV exposure time and interval (Fig. 3.11). I stimulated wild-type cells expressing mRFP-LimEΔcoil two times, where the first stimulus period was variable and the second one was constant. As the first stimulus became longer, the cytosolic responses of F-actin to the second stimuli became weaker at 21-sec intervals (Fig. 3.11A). This finding suggests that the refractory period depends on the stimulus strength. Additionally, the response at 36-sec intervals did not become weaker however long the first stimulus (Fig. 3.11A), consistent with the intracellular cGMP concentration recovering to the basal level within 30 sec [54], [56]. Moreover, I observed F-actin response in *gbpAΔ* cells to confirm cGMP effect on the refractory period. At 21-sec interval stimuli, the decline of the responsiveness was more significant in *gbpAΔ* cells and recovered in rescued *gbpAΔ* cells (Fig. 3.11B). Overall, these results indicate that the cGMP level determines the refractory period for the excitable system composed of sGC and F-actin.

Figure 3.11

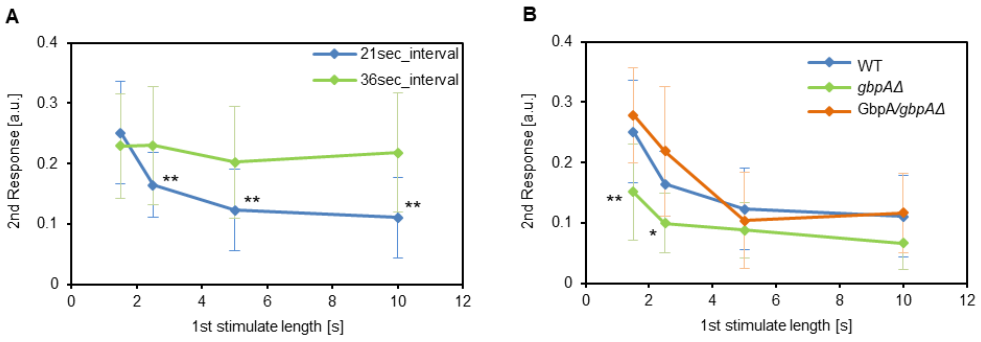

Fig. 3.11 Intracellular cGMP is important for deciding the refractory period.
(A) The repetitive response of F-actin is dependent on the first stimulation length. Wild-type AX3 cells expressing mRFP-LimEΔcoil were stimulated with various lengths of the first stimulus and a 1.5-s second stimulus (mean ± s.d. for at least 16 cells; ** $P < 0.001$, t-test). The cytosolic response was normalized by the maximum fluorescence value (F.I.) in the time course. (B) The indicated cell lines were repeatedly stimulated at 21-s intervals (mean ± s.d. for at least 16 cells; ** $P < 0.001$, * $P < 0.05$ versus wild-type and GbpA, t-test).

Next I investigated the effects of cGMP-GbpC signaling on pseudopod formation in response to cAMP stimulation (Fig. 3.12). Wild-type cells showed transient F-actin polymerization at the entire cell surface at around 10 sec after a stepwise cAMP stimulation, followed by the formation of multiple pseudopods with F-actin polymerization for around 1 min, as observed by the mRFP-LimEΔcoil localization. When *gbpAΔ* cells were exposed to the same stimulus, the same responses were not observed over the several-minute observation period, showing a long suppression of F-actin polymerization (Fig. 3.12A, B). The times for new pseudopods to form after cAMP stimuli were 1.18 ± 0.42 min in wild-type and 5.64 ± 1.92 min in *gbpAΔ* cells (Fig. 3.12D). The cell areas of the pseudopods in the two cell types had similar dynamics (Fig. 3.12C), suggesting that intracellular cGMP is important for regulating the pseudopod formation and cell migration. The ectopic expression of GbpA in *gbpAΔ* cells rescued the delay of the secondary response (Fig. 3.12A, B and D). Furthermore, I observed that *gcΔ* and *gbpCΔ* cells had impaired cGMP-GbpC signaling. Both cells exhibited enhanced F-actin polymerization with little rest (Fig. 3.12A, B and D). These results are consistent with cGMP-GbpC signaling suppressing F-actin polymerization and regulating refractoriness (Fig. 3.9 and 3.10). Thus, the negative regulation from cGMP-GbpC determines the refractory period of the sGC and F-actin localizations and regulates the time scale of pseudopod dynamics.

Fig. 3.12

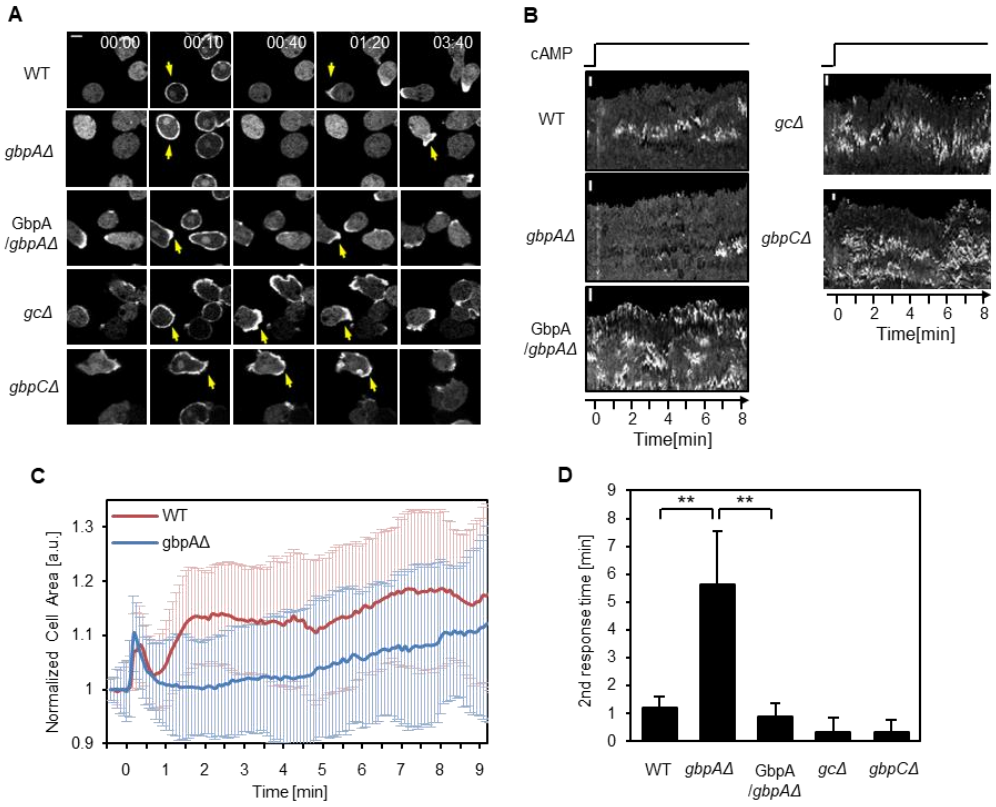

Fig. 3.12 Pseudopod dynamics depends on intracellular cGMP concentration.
(A) Wild-type AX3 and mutant cell lines expressing mRFP-LimEΔcoil were stimulated with 10 nM cAMP. Yellow arrows show the pseudopods where mRFP-LimEΔcoil localized. Time format is mm:ss.
(B) The temporal dynamics of pseudopod formation upon cAMP step stimuli. Kymographs of wild-type AX3 and mutant cell lines were drawn by measuring the fluorescence intensity around the boundary of the cells expressing mRFP-LimEΔcoil in (A). Scale bars: 5 μm.
(C) The cell area of wild-type and *gbpAΔ* cells were normalized by the pre-stimulus level (mean ± s.d. for n = 30 and 37 cells, respectively).
(D) The second response time represents the time required for secondary pseudopod formation after 10 nM cAMP stimulation at time 0 in (A) (mean + s.d. forat least 40 cells; **P<0.001, t-test).

3.2.3 Positive feedback mechanism between sGC and F-actin

Another required mechanism for excitability is the positive feedback loop. I showed that sGC localization and F-actin are incorporated into one excitable network, because sGC localization depends on F-actin (Fig. 3.4) and cGMP-GbpC suppress actin polymerization (Fig. 3.8). If sGC functions to polymerize or stabilize F-actin, then a positive feedback loop is suggested. A previous report has shown that the N-terminus and C-terminus domains of sGC are required for the co-localization with F-actin and stabilization of the pseudopod of the cell, respectively [57]. Although that study showed the stabilization mechanism of F-actin, it did not show if sGC directly interacts with F-actin, because neither domain has conserved regions for binding to F-actin. Therefore, I examined the interaction between sGC and F-actin *in vitro*. I purified sGC-GFP-Flag (sGC-GFPF) and control Flag-Flag-GFP (F_2GFP) proteins from *Dictyostelium* cells while F-actin was prepared from rabbit skeletal muscle (see Methods). Purified proteins were added to a solution containing F-actin labeled with Rh-Ph (Rh-Ph/F-actin) and observed under a fluorescence microscope. F_2GFP as the control protein showed no obvious localization with F-actin (Fig. 3.13A). However, the sGC-GFPF signal overlapped with F-actin strongly, and a structural change of F-actin was observed. Such an F-actin network was reported previously when α-actinin, an F-actin crosslinking protein, was mixed with F-actin [12]. This result suggests that sGC might not only bind to F-actin but also crosslinks the filaments because purified F-actin solution hardly contains actin binding proteins. Next I also tested the binding of the sGC_N and sGC_C domains to F-actin (Fig.3.14B). In the presence of F-actin, purified sGC_N-GFPF and sGC_C-GFPF proteins showed the same complex structure as sGC-GFPF. This result suggests that each domain has multiple actin binding domains for F-actin.

Fig. 3.13

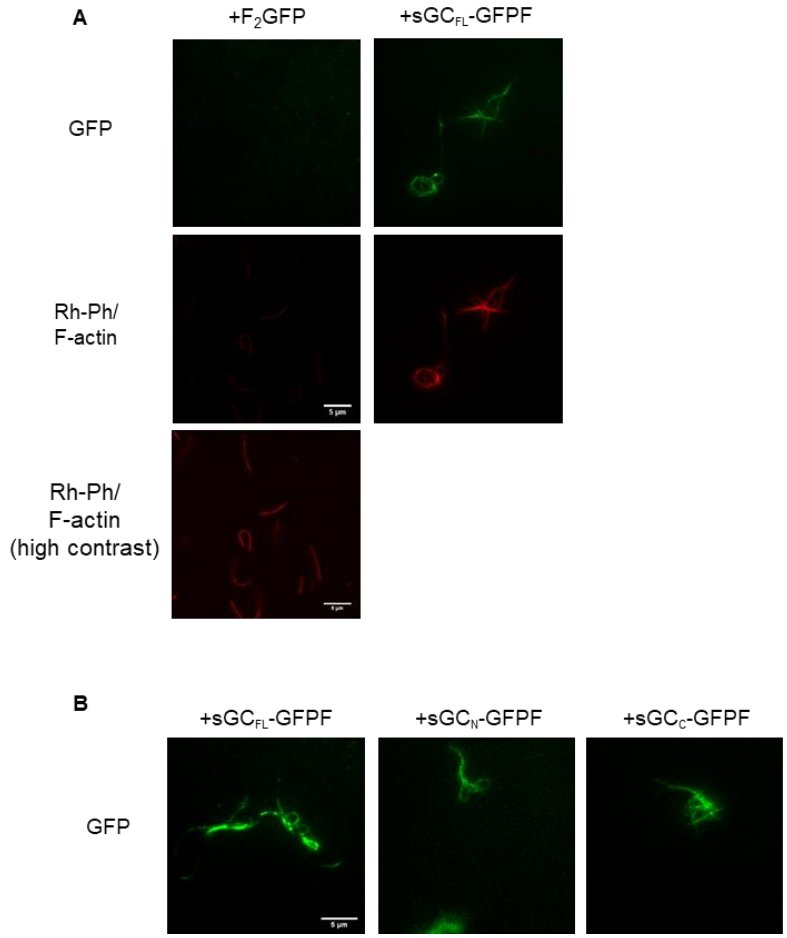

Fig. 3.13 sGC protein interacts with F-actin *in vitro*.
(A) Purified F_2GFP (Flag-Flag-GFP) and sGC_{FL}-GFPF (sGC-GFP-Flag) proteins were mixed with F-actin (purified from Rabbit muscle acetone powder) labeled with Rhodamine-Phalloidin (Rh-Ph/F-actin).
(B) The indicated proteins were mixed with F-actin as shown in A.
Scale bars: 5 μm.

Dictyostelium cells are known to have several F-actin crosslinking proteins such as α-actinin, p-34 and filamin [46]. The F-actin crosslinking activity of α-actinin and p-34 is inhibited by a few μM of calcium, while that of filamin is calcium insensitive. I examined whether the crosslinking activity in the presence of sGC-GFPF is dependent on calcium (Fig. 3.14A). Adding 2 mM $CaCl_2$ to a solution of 1 mM EGTA (free $[Ca^{2+}]\simeq 997$ μM vs. 6.8 nM) had no effect on the F-actin complex network, indicating this crosslinking activity is independent of calcium concentration. Moreover, I observed sGC localization in cells lacking α-actinin, filamin and severin (*abpACΔsevAΔ*) [46]. sGC_N-Halo7 showed strong localization at the surface of these mutant cells (Fig. 3.14B). These data suggest that sGC can bind to and crosslink F-actin directly, resulting in stabilization of the pseudopod. Such a molecular mechanism produces positive feedback between sGC and F-actin.

Fig. 3.14

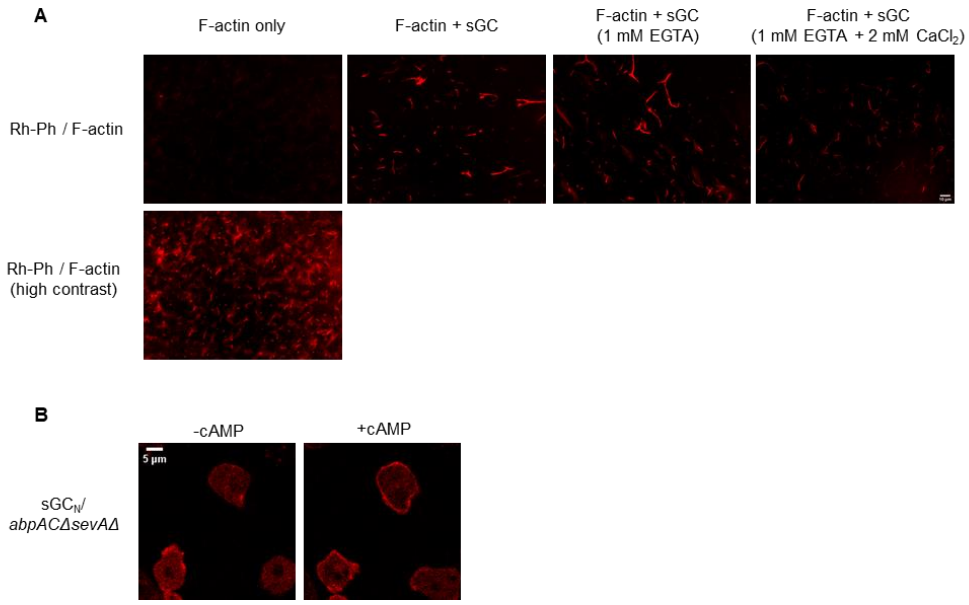

Fig. 3.14 sGC interacts with F-actin directly.
(A) Purified sGC_{FL}-GFPF (sGC-GFP-Flag) protein was mixed with F-actin labeled with Rhodamine-Phalloidin (Rh-Ph/F-actin) in low $[Ca^{2+}]$ (1 mM EGTA + 0 mM $CaCl_2$) or high $[Ca^{2+}]$ (1 mM EGTA + 2 mM $CaCl_2$).
(B) sGC_N-Halo7-expressing cells lacking three actin binding proteins (α-actinin, filamin and severin) were stimulated by 1 μM cAMP.
Scale bar: 5 μm.

3.3 Multiple excitable pathways for efficient migration

3.3.1 Spontaneous cell migration

I showed cell has multiple compasses with different time scales to cAMP stimulus (Fig. 3.5). To address how parallel pathways regulate cell migration, I observed the localization patterns of sGC and PIP3 simultaneously in individual cells. In wild-type cells co-expressing sGC_N-Halo7 and PH_{PKB}-GFP, sGC_N signals were observed in all pseudopods, while PIP3 signals were observed in only half (Fig. 3.15A, B). PIP3 signals were observed in the membrane of pseudopods and inner vesicles, consistent with previous report [61]. Statistical analysis revealed that the localization pattern in pseudopods was classified into three types: pseudopods with sGC_N localization alone (47.8%), with sGC_N and PIP3 co-localization (50.2%) and with PIP3 alone (2.0%) (n = 452 pseudopods from 13 cells) (Fig. 3.15C).

Fig. 3.15

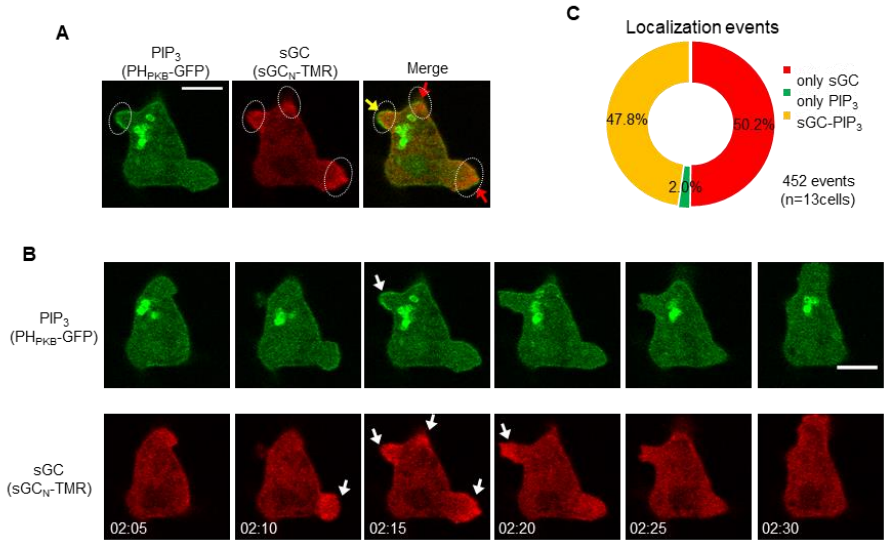

Fig. 3.15 The localization of PIP3 and sGC in spontaneous cell migration.
(A) Representative pseudopods with sGC localization alone (red arrow) or sGC and PIP3 co-localization (yellow arrow) are shown by dotted circles. sGC and PIP3 in a wild-type AX2 cell were visualized by expressing sGC_N–TMR and PH_{PKB}–GFP, respectively.
(B) The time evolution of the pseudopod dynamics shown in (A). sGC and PIP3 localizations are indicated by the white arrows. Time format is mm:ss. Scale bar: 5 μm.
(C) Fraction of pseudopods with sGC, PIP3, or both sGC and PIP3 localization were quantified and shown in the pie chart.

Each localization pattern had different characteristics: pseudopods with sGC and PIP3 co-localization had larger extensions, while small extensions were observed in pseudopods with sGC localization alone (Fig. 3.16A). I analyzed several parameters of the pseudopod dynamics including elongation length, lifetime, contribution to cell movement, and appearance frequency for each localization pattern by measuring the extended area of the spontaneously formed pseudopods (see Methods and Fig. 3.16B, C). The elongation length of the pseudopods with sGC and PIP3 co-localization (5.22 ± 2.31 μm, n= 189 pseudopods) was higher than that of sGC localization alone (3.92 ± 1.79 μm, n= 147 pseudopods) (Fig. 3.16B). Consistently, the lifetime and the contribution to cell motility of the pseudopods with both signals were higher than those with sGC alone, however, the appearance frequency was not significantly different (Fig. 3.16C). Moreover, sGC and PIP3 showed spatially a bit misalignment in the same pseudopod (Fig. 3.16A), which is supported by the fact that sGC co-localizes with F-actin and PIP3 exists in the plasma membrane. To see the sole effect of sGC localization on the pseudopod dynamics, I used sGCΔN-Halo7/*sgcΔ* cells, which express a mutant sGC lacking its N-terminal region but maintains its catalytic domain for cGMP synthesis (Fig. 3.16B). PIP3-alone pseudopods in these mutant cells exhibited small elongations compared to sGC and PIP3 co-localized pseudopods (4.28 ± 2.16 μm, n= 61 pseudopods). Similarly, wild-type cells treated with LY294002, a pharmacological PI3K inhibitor, exhibited sGC-alone pseudopods with only small elongations (2.82 ± 1.08 μm, n= 39 pseudopods) (Fig. 3.16B). These genetic and pharmacological inhibitions also caused defects in the cell motility (Fig. 3.16D, E). Similar decreases in the cell velocity were observed by the inhibition of PIP3 or sGC, and a larger decrease was observed by the inhibition of both pathways (Fig. 3.16E). These observations suggest that the two parallel pathways regulate pseudopod formation additively.

Fig. 3.16

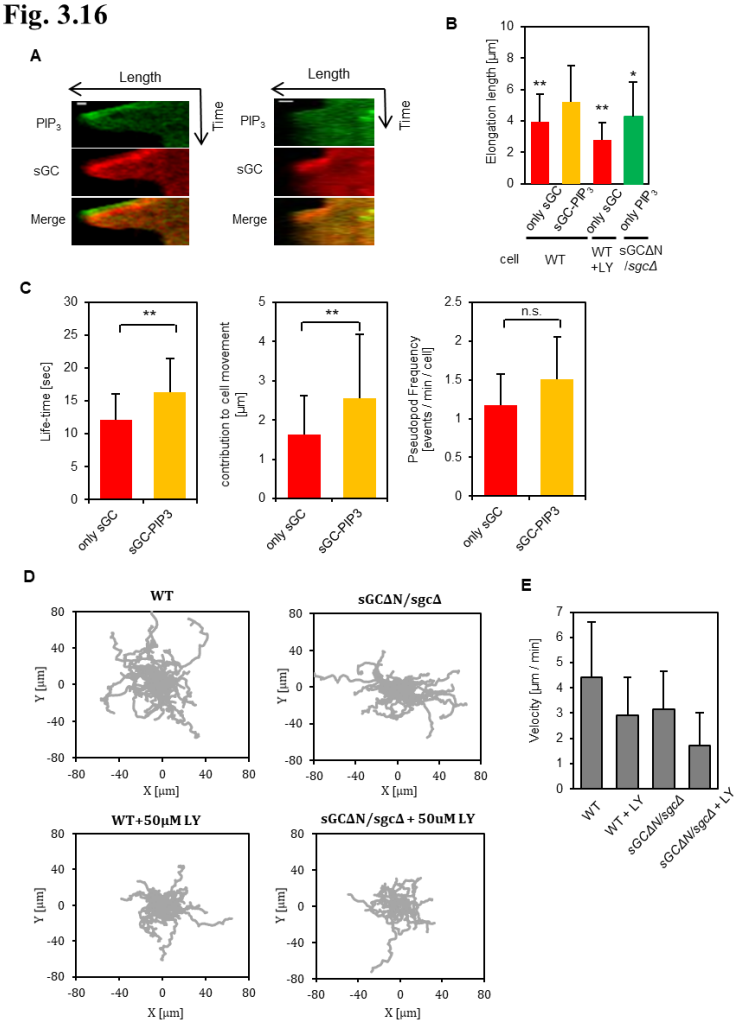

Fig. 3.16 Parallel pathways regulate cell motility additionally.
(A) Pseudopod elongations with the localization of sGC_N–TMR and PH_{PKB}–GFP (left) or sGC_N-TMR alone (right) are shown. The temporal dynamics of sGC_N–TMR and PH_{PKB}–GFP during pseudopod elongation are shown in kymographs (total times shown are 150 s in the left and 200 s in the right). The bottom surface of a cell was observed by confocal microscopy at 5-s intervals. Scale bars: 1 μm.
(B) The elongation length of sGC-localized or sGC- and PIP3-colocalized pseudopods were measured in wild-type AX2 cells. sGC_N-TMR localization in AX2 cells treated with 30 μM LY294002 and PH_{PKB}–GFP localization in *sgcΔ* expressing sGCΔN–Halo7 are also shown. Results are the mean + s.d. for at least 39 pseudopods; *P<0.05, **P<0.001 versus sGC-PIP3 (Bonferroni test). Spontaneous migration of each cell was recorded for 5–10 min.
(C) The lifetime, contribution to cell movement and frequency of the pseudopods with sGC alone or with the co-localization of sGC and PIP3 (mean + s.d. for n = 147 and 189 pseudopods, respectively). The number of pseudopods was counted only if the elongation area was over 4 μm^2 (mean + s.d. for n = 13 cells; **P<0.01, t-test).
(D) The indicated cell lines were observed under an inverted microscope (see Methods) for 20 min, and the coordinates of the cells were analyzed by laboratory-developed software.
(E) The cell velocity was calculated by a change in the coordinates in (D) (mean + s.d. for at least 51 cells).

3.3.2 Pseudopod dynamics under cAMP gradients

I next observed both signaling molecules under cAMP gradients to see how their pathways regulate pseudopod formation in chemotaxis. Particularly, I focused on response time scale by using removable cAMP source because PIP3 and sGC have different length of refractory period. When the source of the chemoattractant gradient was continuously moved around the cell, sGC and PIP3 were able to follow the changes of the position similarly (Fig. 3.17A). These responses are consistent with the refractory periods, because it has been considered that the refractory period is installed in every tiny compartment of the membrane like action potential. On the other hand, once the source position was fixed, the membrane localizations of sGC and PIP3 behaved differently (Fig. 3.17B). The stimulus at first induced sGC and PIP3 localization at the same pseudopod, followed by the disappearance of both signals. Later, sGC localization preceded PIP3 localization on the pseudopod, showing that sGC localized to the pseudopod more frequently than PIP3, consistent with the observations in randomly moving cells and the refractory periods of the two excitable pathways (Fig. 3.16 and 3.5). These results demonstrate that both signaling pathways have their own unique dynamics to the same cAMP stimulation. Each excitable pathway works in parallel, and the cell is able to make a greater displacement when the two pathways couple.

Fig. 3.17

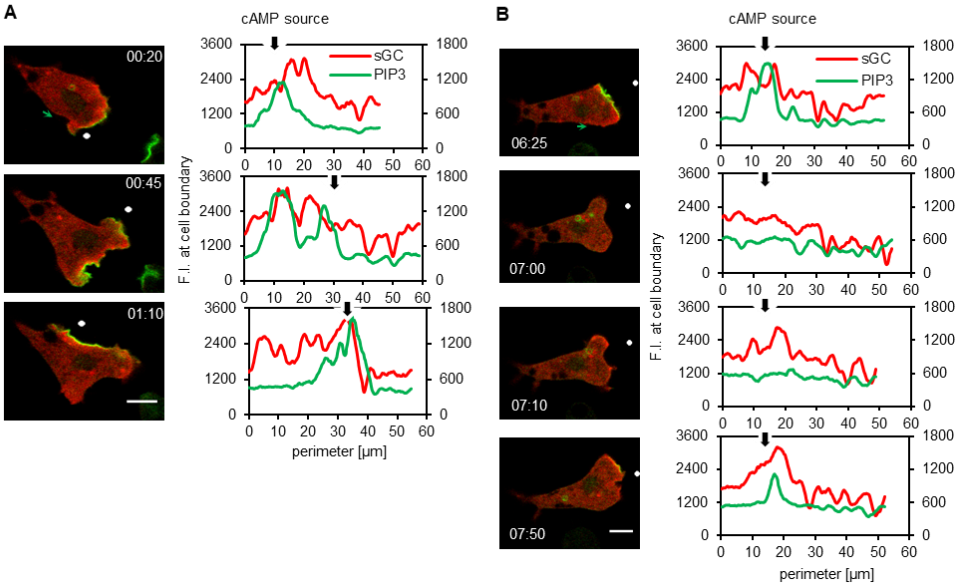

Fig. 3.17 Parallel pathways react to the cAMP gradient with their own refractory periods.
(A, B) The temporal responsiveness of sGC_N–TMR and PH_{PKB}–GFP to a cAMP gradient. The position of a pipette containing 40 nM cAMP is shown by the white dots in the pictures and black arrows in the profiles. The position of the pipette was moved in A and fixed in B. The fluorescence intensity (F.I.) of sGC and PIP3 along the cell surface was measured starting from the positions of the green arrows in the upper cell images. Time format is mm:ss. Scale bars: 5 µm.

Chapter 4
Discussion

4.1 Parallel excitable pathways in eukaryotic cells

Eukaryotic chemotaxis is mediated by parallel signaling pathways, some of which have characteristic features of so-called excitability for the generation of all-or-none signals to regulate pseudopod dynamics at the front of the cells [8], [10]. Although an excitable system does not have the strict definition, previous reports have demonstrated PIP3 excitation on the membrane during the chemotactic signaling of *Dictyostelium* cells and neutrophil cells [19], [37], [50], suggesting that the excitability of the chemotactic signaling pathway has commonality in eukaryotic cells.

Here I demonstrated sGC localization at the cell surface and also showed excitable behaviors such as an all-or-none response (Fig. 3.1), wave-like pattern formation (Fig. 3.3) and refractory period (Fig. 3.2 and 3.5). These observations indicate the universality of excitable systems for chemotactic signaling pathways. Although both the PIP3 and sGC pathways have excitable properties, each pathway independently forms an excitable network, as shown by the following facts. First, sGC localization strongly depends on F-actin (Fig. 3.3), but F-actin is not essential for PIP3 excitation on the membrane [1]. Second, sGC responses upon pulse stimuli showed shorter refractory periods (10 ~ 20 sec) than PIP3 responses (30 ~ 60 sec) (Fig. 3.5). Finally, the refractory period of sGC localization was independent of PIP3 production (Fig. 3.5). These results indicate that each downstream pathway has unique characteristics for excitable dynamics. These findings revealed that sGC localized to the pseudopod more frequently than PIP3 when cells moved along the chemoattractant gradient (Fig. 3.17). Under constant chemical gradients, it took 10~30 sec for sGC to re-localize to the pseudopod once the localization disappeared, which is consistent with the refractory periods seen for sGC responses to pulse stimuli (Fig. 3.2). These results suggest that the refractory period for the localization of a signaling molecule corresponds to the frequency of the pseudopod formation.

Although a cAMP stimulus induces PIP3 and sGC excitation on the cell

surface independently (Fig. 3.4), there may be crosstalk between these pathways. Previous studies showed that F-actin is required for PI3K localization at the pseudopod and that the positive feedback comprising of Ras, PI3K and F-actin is important for directional cell migration [42]. Additionally, I showed that sGC localization strongly depends on F-actin dynamics (Fig. 3.3) and sGC would stabilize F-actin structure (Fig. 3.13). These observations suggest positive feedback between the PI3K-PTEN and sGC pathways through F-actin dynamics. This crosstalk could control pseudopod dynamics positively and cooperatively. I further found that pseudopods have different molecular fingerprints (Fig. 3.15). Spontaneously moving cell exhibited pseudopods with sGC localization and with both sGC and PIP3 localization, while pseudopods with only PIP3 localization were rarely observed. Pseudopod analysis revealed that these two types of pseudopods differ. The localization of both sGC and PIP3 extends pseudopods more extensively than the localization of either alone (Fig. 3.16). Additionally, the lifetimes and contribution to cell movement are longer and bigger. The crosstalk between PI3K-PTEN and sGC pathways could produce the extended pseudopod.

An excitable pathway works as the internal compass for cell migration [37], [45]. In my doctoral research, I showed multiple pathways with the excitable characteristics regulates pseudopod formation. Simultaneous observation of PIP3 and sGC in a single cell revealed that each pathway induces pseudopod formation, and moreover, co-localization of them extended pseudopods greater (Fig. 3.16). Additionally, multiple pathways have the different refractory period (Fig. 3.5). These results suggest that multiple internal compasses with the different time scale regulate chemotaxis (Fig. 4.1). Each pathway responds to the environmental change, and the greater extension is occurred when the direction of two compasses couple. Combination of the different time scale may enable cell to respond to the complicated change in the environment. However, the contribution for parallel pathways to chemotaxis is unknown. It is important to demonstrate PIP3 and sGC localizations in physiologically conditions.

Fig. 4.1

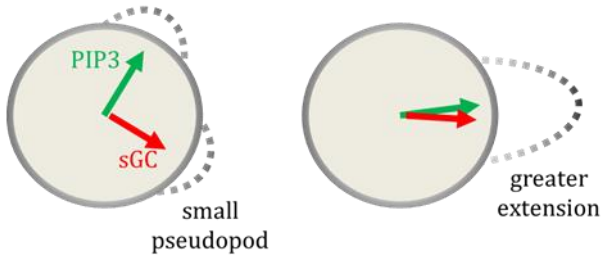

Fig. 4.1 The scheme for pseudopod extension.
Excitable pathways including PIP3 and sGC work as the internal compass of cell migration in parallel. Each compass induces small pseudopod formation (left). When the direction of two compasses are same, cell produce pseudopod with grater extension (right).

4.2 cGMP signaling regulates pseudopod formation

The idea that the short refractory pseudopod regulated by sGC pathway was supported from following observations. The refractory period of F-actin depends on the duration of the first pulse stimulus and is less than 36 sec (Fig. 3.11), consistent with the cGMP dynamics produced by cAMP stimuli [54], [56]. Additionally, *gbpAΔ* cells lacking cGMP degradation activity showed prolonged refractoriness and prolonged suppression of F-actin polymerization and pseudopod formation (Fig. 3.10 and 3.12) [35], [39]. The prolonged refractoriness has been reported also in *gbpAΔ* cells in response to light-scattering or Ca^{2+} influx upon a cAMP stimulus [32]. These data suggest that the modulation of intracellular cGMP concentration affected the refractory period in sGC/F-actin responses and pseudopod formation. Furthermore, two cGMP signaling-deficient cell lines, *gcΔ* and *gbpCΔ* cells, showed pseudopod formation more frequently than wild-type cells (Fig. 3.12). Also, *gbpCΔ* cells have no obvious refractory period (Fig. 3.9). These data indicate that cGMP signaling regulates the negative feedback regulation component of the excitability of the sGC/F-actin dynamics.

It has been reported that when stimulated twice at 30 sec intervals, cells synthesize cGMP upon the first stimulus but not upon the second, indicating some form of adaptation [54]. That same report showed that the addition of a cAMP phosphodiesterase enabled cGMP production in response to both stimuli. These results suggest that cGMP could be produced repetitively when cAMP stimulation is short enough so as to avoid complete adaptation. In my doctoral thesis, the optical uncaging experiments stimulated cells before complete recovery from the first excitation and therefore cell would produce cGMP repetitively by pulse stimuli. Furthermore, the refractory period of F-actin itself was dependent on the duration of the pulse stimulus (Fig. 3.11), which is the previous report that the amount of produced cGMP depends on the stimulus strength [56]. Based on these observations, I suggest that the refractory period regulated by cGMP-dependent GbpC signaling is a physiologically important feature for chemotactic cell migration. However, it is unclear whether cGMP suppresses pseudopod formation during spontaneous migration and chemotaxis. To understand pseudopod regulation mechanism, it is important to observe the intracellular cGMP dynamics.

Previous studies have also shown that cGMP and GbpC signaling activation

induces pseudopod suppression at the rear end of cells via the regulation of myosin II [6], [57]. On the other hand, it is known that myosin II is not essential for the retraction of the anterior pseudopod observed in *mhcA∆* cells [20]. Similarly, I found myosin II was not essential for sGC/F-actin association to and dissociation from the cell surface (Fig. 3.7 and 3.8). Taken together, cGMP-dependent GbpC signaling could serve for anterior retraction of the pseudopod, with myosin II making only a minor contribution.

4.3 Molecular mechanisms producing excitability

An excitable system requires positive and negative feedback loops for the response. cGMP-GbpC signaling would regulate the negative feedback for sGC excitability. As for the positive feedback regulation, it was predicted that PIP3 accelerates PTEN dissociation from the cell membrane [45]. PTEN dissociation results in the accumulation of PIP3 on the membrane, providing the positive feedback mechanism. In the sGC pathway, whether sGC activates actin polymerization or stabilizes the F-actin structure is unclear, because sGC has no conserved actin binding domains [57].

Here I investigated the possible mechanism for positive feedback regulation between sGC and F-actin by mixing purified proteins *in vitro*. As a result, fluorescently tagged sGC and F-actin showed strong co-localization and a stabilized structure (Fig. 3.13). This phenomenon indicates that sGC crosslinks and stabilizes F-actin. Moreover, the N- and C-termini of sGC showed identical function, suggesting that sGC has numerous actin binding domains in a single protein. This hypothesis was supported by the Ca^{2+} independence of the F-actin stabilization and sGC localization in cells lacking major actin crosslink proteins (Fig. 3.14). These data suggest that sGC crosslinks F-actin directly and stabilizes the pseudopod during spontaneous and chemotactic cell migration. However, my data is not enough for the proof that F-actin crosslink activity by sGC produces the positive feedback between sGC and F-actin. Further investigations including biochemical assay and mathematical analysis are needed.

4.4 A plausible model for sGC localization regulation

Schematic model of sGC localization is summarized as a scheme in Fig. 4.2. Chemoattractant stimulation triggers sGC translocation to F-actin on the cell

surface. sGC stabilizes F-actin, which induces further sGC localization to the cell surface. This positive feedback regulation enables all-or-none response for sGC localization. At the same time, sGC catalyzes cGMP production upon the chemoattractant stimulation [40]. The produced cGMP binds to GbpC directly and induces its kinase activation through a series of intramolecular signals. Then it initiates the destabilization of F-actin and sGC dissociation from the cell surface. The negative feedback signaling suppresses further pseudopod elongation and induces pseudopod retraction. In my scheme, cGMP-dependent GbpC signaling defines the refractoriness in sGC excitability, which is linked to suppression of the pseudopod. It has been previously reported that GbpC provides major intracellular cGMP binding sites at a high affinity (Kd = around 10^{-9} M) and slow dissociation rate (half-life of ~ 2 min) [53]. The kinetics disagree with my model, which assumes a much faster dissociation for cGMP of 20-30 sec. This evidence suggest certain aspects of the mechanism are missing from my model. For example, an unknown factor with low affinity and fast dissociation to cGMP might function downstream of the cGMP-GbpC complex or partial activation of this complex might be enough for repetitive normal responses. Future work is needed to clarify how cGMP regulates F-actin suppression through GbpC.

Fig. 4.2

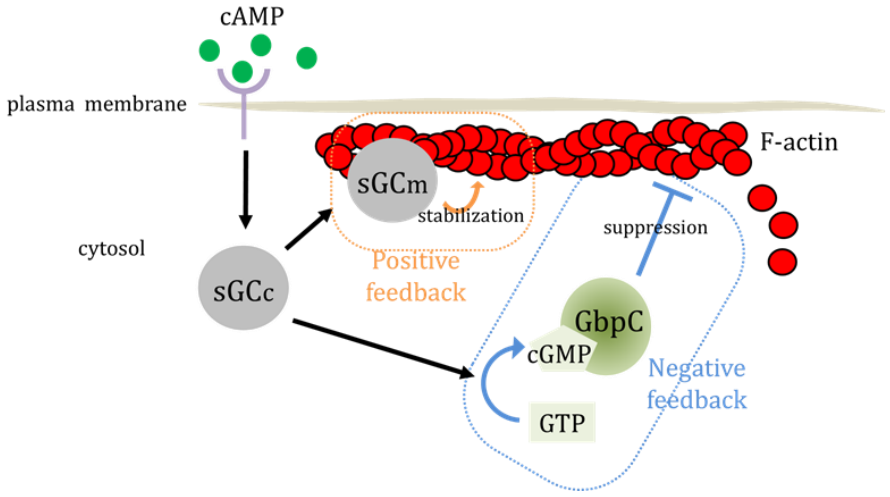

Fig. 4.2 A model illustrating the sGC excitable system.
cAMP stimulation induces sGC localization via actin polymerization and cGMP production by the catalytic activity of sGC. sGC stabilizes the F-actin structure at the front of the cell. Simultaneously, the synthesized cGMP binds to GbpC to inhibit sGC localization through actin depolymerization.

Bibliography

[1] Arai, Y., Shibata, T., Matsuoka, S., Sato, M. J., Yanagida, T. and Ueda, M. (2010). Self-organization of the phosphatidylinositol lipids signaling system for random cell migration. *Proc. Natl. Acad.Sci*. USA. **107**, 12399-12404

[2] Artemenko, Y., Lampert, T. J. and Devreotes, P. N. (2014). Moving towards a paradigm: Common mechanism of chemotactic signaling in *Dictyostelium* and mammalian leukocytes. *Cell Mol. Life Sci.* **71**, 3711-3747

[3] Asano, Y., Nagasaki, A. and Uyeda, T. Q. P. (2008). Correlated waves of actin filaments and PIP3 in *Dictyostelium* cells. *Cell Motil. Cytoskeleton* **65**, 923-934

[4] Beta, C., Wyatt, D., Rappel, W. J. and Bodenschatz, E. (2007). Flow photolysis of spatiotemporal stimulation of single cells. *Anal. Chem.* **79**, 3940-3944

[5] Bosgraaf, L., Russcher, H., Smith, J. L., Wessels, D., Soll, D. R. and Van Haastert, P. J. M. (2002). A novel cGMP signaling pathway mediating myosin phosphorylation and chemotaxis in *Dictyostelium*. *EMBO J.* **21**, 4560-4570

[6] Bosgraaf, L., Waijer, A., Engel, R., Visser, A. J. W. G., Wessels, D., Soll, D. and Van Haastert, P. J. M. (2005). RasGEF-containing proteins GbpC and GbpD have differential effects on cell polarity and chemotaxis in *Dictyostelium*. *J. Cell Sci*. **118**, 1899-1910

[7] Bosgraaf, L. and Van Haastert, P. J. M. (2009). Navigation of chemotactic cells by parallel signaling to pseudopod persistence and orientation. *PLoS ONE* **4**, e6842

[8] Cai, H. and Devreotes, P. N. (2011). Moving in the right direction: How eukaryotic cells migrate along chemical gradients. *Semin. Cell Dev. Biol.* **22**, 834-841

[9] Cao, Y., Lopatkin, A. and You, L. (2016). Elements of biological oscillations in time and space. *Nat. Struct. Mol. Biol*. **23**, 1030-1034

[10] Devreotes, P. N., Bhattacharya, S., Edwards, M., Iglesias, P. A., Lampert, T. and Miao, Y. (2017). Excitable signal transduction networks in directed cell migration. *Annu. Rev. Cell Dev. Biol.* **33**, 103-125

[11] Devreotes, P., N. and Horwitz, A., R. (2015). Signaling networks that regulate cell migration. *Cold Spring Harb. Perspect. Biol*. **7**, a005959

[12] Falzone, T. T., Lenz, M., Kovar, D. R. and Gardel, M. L. (2012). Assembly kinetics determine the architecture of α-actinin crosslinked F-actin networks. *Nat. Commun*. **3**, 861

[13] Fischer, M., Haase, I., Simmeth, E., Gerisch, G. and Muller-Taubenberger, A. (2004). A brilliant monomeric red fluorescent protein to visualize cytoskeleton dynamics in *Dictyostelium*. *FEBS Lett.* **577**, 227-232

[14] Gerisch, G., Ecke, M., Wischnewski, D. and Schroth-Diez, B. (2011). Different modes of state transitions determine pattern in the phosphatidylinositide-actin system. *BMC Biol*. **12**, 42

[15] Gerisch, G., Schroth-Diez, B., Muller-Taubenberger, A. and Ecke, M. (2012). PIP3 waves and PTEN dynamics in the emergence of cell polarity. *Biophys. J*. **103**, 1170-1178

[16] Goldberg, J. M., Bosgraaf, L., Van Haastert, P. J. M. and Smith, J. L. (2002). Identification of four candidate cGMP targets in *Dictyostelium*. *Proc. Natl. Acad. Sci*. USA. **99**, 6749-6754

[17] Hilborn, R. C., Brookshire, B., Mattingly, J., Purushotham, A. and Sharma, A. (2012). The transition between stochastic and deterministic behavior in and excitable gene circuit. *PLoS ONE* **7**, e34536

[18] Hind, L. E., Vincent, W. J. B. and Huttenlocher, A. (2016). Leading from the back: the role of the uropod in neutrophil polarization and migration. *Dev. Cell* **38**, 161-169

[19] Huang, C. H., Tang, M., Shi, C., Iglesias, P. A. and Devreotes, P. N. (2013). An excitable signal integrator couples to an idling cytoskeletal oscillator to drive cell migration. *Nat. Cell Biol.* **15**, 1307-1316

[20] Iwadate, Y. and Yumura, S. (2008). Actin-based propulsive forces and myosin-II-based contractile forces in migrating *Dictyostelium* cells. *J. Cell Sci.* **121**, 1314-1324

[21] Iijima, M. and Devreotes, P. (2002). Tumor suppressor PTEN mediates sensing of chemoattractant gradients. *Cell* **109**, 599-610

[22] Kalil, K. and Dent, E. W. (2005). Touch and go: guidance cues signal to the growth cone cytoskeleton. *Curr. Opin. Neurobiol.* **15**, 521-526

[23] Kamimura, Y., Xiong, Y., Iglesias, P. A., Hoeller, O., Bolourani, P. and Devreotes, P. N. (2008). PIP_3-independent activation of TorC2 and PKB at the cell's leading edge mediates chemotaxis. *Curr. Biol.* **18**, 1034-1043

[24] Kamimura, Y., Miyanaga, Y. and Ueda, M. (2016). Heterotrimeric G-protein shuttling via Gip1 extends the dynamic range of eukaryotic chemotaxis. *Proc. Natl. Acad. Sci*. USA. **113**, 4356-4361

[25] Khamviwath, V., Hu, J. and Othmer, H. G. (2013). A continuum model of actin waves in *Dictyostelium discoideum*. *PLoS ONE* **8**, e64272

[26] Kortholt, A., Rehmann, H., Kae, H., Bosgraaf, L., Keizer-Gunnink, I., Weeks, G., Wittinghofer, A. and Van Haastert, P. J. M. (2006). Characterization of the GbpD-activated Rap1 pathway regulating adhesion and cell polarity in *Dictyostelium discoideum*. *EMBO J.* **281**, 23367-23376

[27] Kortholt, A., Kataria, R., Keizer-Gunnink, I., Van Egmond, W. N., Khanna, A. and Van Haastert, P. J. M. (2011). *Dictyostelium* chemotaxis: essential Ras activation and accessory signaling pathways for amplification. *EMBO Rep.* **12**, 1273-1279

[28] Kuwayama, H., Ishida, S. and Van Haastert, P. J. M. (1993). Non-chemotactic *Dictyostelium discoideum* mutants with altered cGMP signal transduction. *J. Cell Biol.* **123**, 1453-1462

[29] Kuwayama, H., Viel, G. T., Ishida, S. and Van Haastert, P. J. M. (1995). Abberant cGMP-binding activity in non-chemotactic *Dictyostelium discoideum* mutants. *Biochim. Biophys. Acta* **1268**, 214-220

[30] Langridge, P. D. and Kay R. R. (2007). Mutants in the *Dictyostelium* Arp2/3 complex and chemoattractant-induced actin polymerization. *Exp. Cell Res.* **313**, 2563-2574

[31] Lan, G., Sartori, P., Neumann, S., Sourjik, V. and Tu, Y. (2012). The energy-speed-accuracy tradeoff in sensory adaptation. *Nat. Phys.* **8**, 422-428

[32] Lusche, D. F. and Malchow, D. (2005). Developmental control of cAMP-induced Ca2+-influx by cGMP: influx is delayed and reduced in a cGMP-phosphodiesterase D deficient mutant of *Dictyostelium discoideum. Cell Calcium* **37**, 57-67

[33] Mayor, R. and Etienne-Manneville, S. (2016). The front and rear of collective cell migration. *Nat. Rev. Mol. Cell Biol.* **17**, 98-109

[34] Meili, R., Ellsworth, C., Lee, S., Reddy, T. B. K., Ma, H. and Firtel, R. A. (1999). Chemoattractant-mediated transient activation and membrane localization of Akt/PKB is required for efficient chemotaxis to cAMP in *Dictyostelium*. *EMBO J.* **18**, 2092-2105

[35] Meima, M. E., Biondi, R. M. and Schaap, P. (2002). Identification of a novel type of cGMP phosphodiesterase that is defective in the chemotactic *stmF* mutants. *Mol. Biol. Cell* **13**, 3870-3877

[36] Nakajima, A., Ishihara, S., Imono, D. and Sawai, S. (2014). Rectified directional sensing in long-range cell migration. *Nat., Commun*. **5**, 5367

[37] Nishikawa, M., Horning, M., Ueda, M. and Shibata, T. (2014).

Excitable signal transduction induces both spontaneous and directional cell asymmetries in the phosphatidylinositol lipid signaling system for eukaryotic chemotaxis. *Biophys. J.* **106**, 723-734

[38] Ori, H., Marder, E. and Marom, S. (2018). Cellular function given parametric variation in the Hodgkin and Huxley model of excitability. *Proc. Natl. Acad. Sci*. USA. **115**, E8211-E8218

[39] Roelofs, J., Meima, M., Schaap, P and Van Haastert, P. J. M. (2001). The *Dictyostelium* homologue of mammalian soluble adenylyl cyclase encodes a guanylyl cyclase. *EMBO. J*. **20**, 4341-4348

[40] Roelofs, J. and Van Haastert, P. J. M. (2002). Characterization of two unusual guanylyl cyclases from *Dictyostelium*. *J. Biol. Chem.* **277**, 9167-9174

[41] Sager, B. M. (1996). Propagation of traveling waves in excitable media. *Genes Dev*. **10**, 2237-2250

[42] Sasaki, A. T., Chun, C., Takeda, K. and Firtel, R. A. (2004). Localized Ras signaling at the leading edge regulates PI3K, cell polarity, and directional cell movement. *J. Cell Biol.* **167**, 505-518

[43] Sato, M. J., Kuwayama, H., van Egmond, W. N., Takayama, A. L. K., Takagi, H., van Haastert, P. J. M., Yanagida, T. and Ueda, M. (2009). Switching direction in electric-signal-induced cell migration by cyclic guanosine monophosphate and phosphatidylinositol signaling. *Proc. Natl. Acad. Sci.* USA. **106**, 6667-6672.

[44] Servant, G., Weiner, O. D., Herzmark, P., Balla, T., Sedat, J. W. and Bourne, H. R. (2000). Polarization of chemoattractant receptor signaling during neutrophil chemotaxis. *Science* **287**, 1037-1040

[45] Shibata, T., Nishikawa, M., Matsuoka, S. and Ueda, M. (2013). Intracellular encoding of spatiotemporal guidance cues in a self-organizing signaling system for chemotaxis in *Dictyostelium* cells. *Biophys. J*. **105**, 2199-2209

[46] Schindl, M., Wallraff, E., Deubzer, B., Witke, W., Gerisch, G. and Sackmann, E. (1995). Cell-substrate interactions and locomotion of Dictyostelium wild-type and mutants defective in three cytoskeletal proteins: A study using quantitative reflection interference contrast microscopy. *Biophys. J.* **68**, 1177-1190

[47] Skoge, M., Wong, E., Hamza, B., Bae, A., Martel, J., Kataria, R., Keizer-Gunnink, I., Kortholt, A., van Haastert, P. J. M., Charras, G., Janetopoulos, C. and Irimia, D. (2016). A worldwide competition to compare the speed and chemotactic accuracy of neutrophil-like cells. *PLoS ONE* **11**, e0154491

[48] Soll, D. R., Wessels, D., Kuhl, S. and Lusche, D. F. (2009). How a cell crawls and the role of cortical myosin II. Eukaryot. *Cell* **8**, 1381-1396

[49] Suel, G. M., Garcia-Ojalvo, J., Liberman, L. M. and Elowitz, M. B. (2006). An excitable gene regulatory circuit induces transient cellular differentiation. *Nat.* **440**, 545-550

[50] Tang, M., Wang, M., Shi, C., Iglesias, P. A., Devreotes, P. N. and Huang, C. H. (2014). Evolutionarily conserved coupling of adaptive and excitable networks mediates eukaryotic chemotaxis. *Nat. Commun.* **5**, 5175

[51] Tweedy, L., Knecht, D. A., Machay, G., M. and Insall, R., H. (2016). Self-generated chemoattractant gradients: Attractant depletion extends the range and robustness of chemotaxis. *PLoS Biol.*, 14, e1002404

[52] Van Egmond, W. N., Kortholt, A., Plak, K., Bosgraaf, L., Bosgraaf, S., Keizer-Gunnink, I. and Van Haastert, P. J. M. (2008). Intramolecular activation mechanism of the *Dictyostelium* LRRK2 homolog Roco protein GbpC. *J. Biol. Chem.* **283**, 30412-30420

[53] Van Haastert, P. J. M., Van Walsum, H., and Pasveer, F. J. (1982). Nonequilibrium kinetics of a cyclic GMP-binding protein in *Dictyostelium discoideum*. *J. Cell Biol.* **94**, 271-278

[54] Van Haastert, P. J. M., and Van Der Heijden. (1983). Excitation, adaptation, and deadaptation of the cAMP-mediated cGMP response in *Dictyostelium discoideum*. *J. Cell Biol.* **96**, 347-353

[55] Van Haastert, P. J. M. and Devreotes, P. N. (2004). Chemotaxis: signaling the way forward. *Nat. Rev. Mol. Biol. Cell* **5**, 626-634

[56] Veltman, D. M., Roelofs, J., Engel, R., Visser, A. J. and Van Haastert, P. J. M. (2005). Activation of soluble guanylyl cyclase at the leading edge during *Dictyostelium* chemotaxis. *Mol. Biol. Cell* **16**, 976-983

[57] Veltman, D. M. and Van Haastert, P. J. M. (2006). Guanylyl cyclase protein and cGMP product independently control front and back of chemotaxing *Dictyostelium* cells. *Mol. Biol. Cell* **17**, 3921-3929

[58] Veltman, D.M. and Van Haastert, P. J. M. (2007). The role of cGMP and the rear of the cell in *Dictyostelium* chemotaxis and cell streaming. *J. Cell Sci*. **121**, 120-127

[59] Veltman, D. M., Keizer-Gunnik, I. and Van Haastert, P. J. M. (2008). Four key signaling pathways mediating chemotaxis in Dictyostelium discoideum. *J. Cell Biol.* **180**, 747-753

[60] Watts, D.J. and Ashworth, J. M. (1970). Growth of myxamoebae of the cellular slime mould *Dictyostelium discoideum* in axenic culture. *Biochem. J.*

119, 171-174
[61] Williams, T. D., Paschke., P. I. and Kay, R. R. (2019). Function of small GTPases in Dictyostelium micropinocytosis. *Philos. Trans. R. Soc. B.* **374**, 20180150
[62] Xiong, Y., Huang, C. H., Iglesias, P. A. and Devreotes, P. N. (2010). Cells navigate with a local-excitation, global-inhibition-biased excitable network. *Proc. Natl Acad. Sci.* USA **107**, 17079-17086

Publication list

Paper

Tanabe, Y., Kamimura, Y. and Ueda, M. (2018). Parallel signaling pathways regulate excitable dynamics differently to mediate pseudopod formation during eukaryotic chemotaxis. *J. Cell Sci.* **131**, jcs214775

Oral presentation

Tanabe, Y., Ueda, M., "走化性を調節する複数経路~PI3K 経路と sGC 経路の関係~" 日本細胞性粘菌学会第 5 回例会, 青森県, 弘前大学, October 2015.

Tanabe, Y., Ueda, M., "走化性シグナル伝達における cGMP 経路の働き" 日本細胞性粘菌学会第 4 回例会, 宮城県, 東北大学, October 2014.

Tanabe, Y., Ueda, M., "細胞性粘菌の走化性を調節する興奮性シグナル伝達経路" 新学術領域 "動く細胞と秩序" 第 4 回若手の会, 熊本県, 火の国ハイツ, September 2014.

Poster presentation

Tanabe, Y., Ueda, M., "Guanylate cyclase mediates chemotaxis by transducing high-frequency signals for pseudopod formation." 第 55 回日本生物物理学会年会, 2Pos141, 熊本県, 熊本大学, September 2017.

Tanabe, Y., Ueda, M., "Excitability of sGC pathway mediating chemotaxis in Dictyostelium cells." 第 69 回日本細胞生物学会大会, P1-076, 宮城県, 仙台国際センター, June 2017.

Tanabe, Y., Ueda, M., "Spatiotemporal different localizations of multiple signaling molecules mediate chemotaxis in Dictyostelium cells." 第 68 回日本細胞生物学会大会, P1-48, 京都府, 京都テルサ, June 2016.

Tanabe, Y., Ueda, M., "走化性を調節するグアニル酸シクラーゼの興奮性回路" 日本細胞性粘菌学会第 6 回例会, 東京都, 上智大学, October 2016.

Tanabe, Y., Ueda, M., "Spatiotemporal different localizations of multiple signaling molecules mediating chemotaxis." P11, Westward Look Resort, Tucson, AZ 85704, USA, July 2016

Tanabe, Y., Ueda, M., “Spatiotemporal different localizations of multiple signaling molecules mediate chemotaxis in Dictyostelium cells.” 第 53 回日本生物物理学会年会, 3Pos212, 石川県, 金沢大学, September 2015

Tanabe, Y., Ueda, M., “Excitability of guanylate cyclase signaling pathway mediating chemotaxis.” 理研シンポジウム「細胞システムの動態と論理 VI」, 埼玉県, 独立行政法人理化学研究所生物科学研究棟, April 2014.

Tanabe, Y., Ueda, M., “Excitability of guanylate cyclase signaling pathway mediating chemotaxis in Dictyostelium cells.” 第 52 回日本生物物理学会年会, 2P224, 北海道, 札幌コンベンションセンター, September 2014.

Tanabe, Y., Ueda, M., “Excitability of guanylate cyclase signaling pathway mediating chemotaxis.” Biophysical Society 58th Annual Meeting, 2644-Pos, Moscone Center, San Francisco, CA, USA, February 2014.

Tanabe, Y., Ueda, M., “走化性シグナル伝達におけるグアニル酸シクラーゼ経路の寄与” 定量生物学の会, P057, 東京都, 東京大学, November 2013.

Acknowledgements

Osaka University
Prof. Masahiro Ueda
Prof. Kenji Matsuno
Prof. Koich Fujimoto
Dr. Jun Kozuka
Mr. Shinichi Yamazaki
Ms. Hitomi Matsubara
Mr. Kazutoshi Takebayashi
Ms. Haruka Hiraoka
Ms. Da Young Shin
Mr. Daisuke Yoshioka
Mr. Tsunenori Ouchida
Mr. Shotaro Numano
Ms. Miri Takayama
Mr. Rin Tanaka
Ms. Ayaka Yagi
Ms. Rie Sumida
Ms. Hiroko Hatagami

RIKEN BDR
Dr. Yoichiro Kamimura
Dr. Satomi Matsuoka
Dr. Michio Hiroshima
Dr. Tatsuo Shibata
Dr. Masato Yasui
Ms. Kaori Tanabe
Ms. Shizuka Taguchi
Ms. Akiko Kanayama
Ms. Sumire Hino

Toho University
Dr. Tetsuya Muramoto

Nara Medical University
Dr. Hiroaki Takagi

University of Hyogo
Dr. Hiroyasu Koteishi

Kyushu Institute of Technology
Dr. Yusuke Morimoto

National Institute of Genetics
Dr. Kayo Hibino

University of Miami
Mr. Pravat Dhakal

Abbott Japan Co., Ltd.
Dr. Yukihiro Miyanaga
Dr. Takamitsu Morikawa
Dr. Tomotaka Komori
Mr. Takuma Degawa

Zido, Ltd.
Dr. Seiya Fukushima

I thank P. Van Haastert for the plasmids expressing the sGC-GFP, sGCΔcat-GFP and GbpC mutants, and National BioResource Project (NBRP)-Nenkin for the AX3, *gbpAΔ, gbpABΔ, gbpCΔ, gbpDΔ, mhcAΔ, gbpACΔsevAΔ* and *mutated arcB* cells. I also appreciate the basic information from DictyBase.
I would like to thank Professor Masahiro Ueda for his suggestions and support for my study. I also thank Dr. Yoichiro Kamimura for his technical advice and support. I would like to express my appreciation to Professors Kenji Matsuno and Koichi Fujimoto for reviewing this paper. I also thank the Japan Society for the Promotion of Science (JSPS) for financial support. Finally, I am grateful to all the members listed above, my friends and family for all their support.